

Chemo- and Stereospecific Solid-State Thermal Dimerization of Sodium *trans*-2-Butenoate and γ -Ray-Induced Single-Crystal-to-Single-Crystal Dimerization of Hexaaquamagnesium *trans*-2-Butenoate Dihydrate: Both Give *rel*-(3*S*,4*R*)-1-Hexene-3,4-dicarboxylate but by Different Mechanisms. Stereospecific γ -Ray-Induced Trimerization of Sodium *trans*-2-Butenoate

Wen Shang, Roxana F. Schlam, Magali B. Hickey, Jingye Zhou, Kraig A. Wheeler, Graciela C. Diaz de Delgado, Chun-Hsing Chen, Barry B. Snider,* and Bruce M. Foxman*



Cite This: *Cryst. Growth Des.* 2021, 21, 663–682



Read Online

ACCESS |



Metrics & More

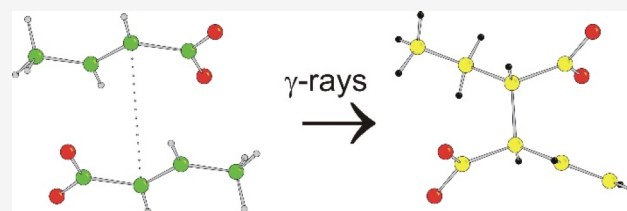


Article Recommendations



Supporting Information

ABSTRACT: γ -Irradiation of crystalline hexaaquamagnesium *trans*-2-butenate dihydrate affords *rel*-(3*S*,4*R*)-1-hexene-3,4-dicarboxylate by a single-crystal-to-single-crystal reaction. The reaction proceeds by a radical chain mechanism with *anti* addition to the butenoate double bond, as established by deuterium labeling. The product structure is that expected from the orientation of *trans*-2-butenates in the pristine crystal. The same dicarboxylate is formed by heating crystalline sodium *trans*-2-butenate at 300 °C, but the thermal ene reaction was shown by deuterium labeling to proceed by *syn* addition to the butenoate double bond as expected for a concerted ene reaction. γ -Irradiation of sodium *trans*-2-butenate forms a single trimer chemo-, regio-, and stereospecifically. The structure of sodium *trans*-2-butenate was determined, and the crystal packing is consistent with both the observed ene dimerization and γ -ray-induced trimerization.



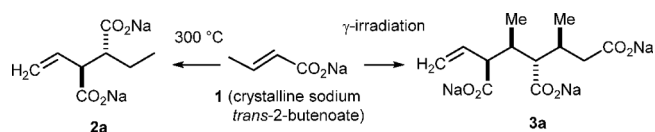
INTRODUCTION

The design and discovery of new classes of materials that undergo solid-state transformations to give products unavailable from solution chemistry and the elucidation of the principles that govern their reactivity remain important challenges in the field.^{1–4} The use of ionizing radiation as an excitation source provides new synthetic opportunities distinct from thermal or photochemical stimuli. ⁶⁰Co γ -rays can initiate radical chain reactions in crystals that lead to products from alkenes very different from those obtained photochemically, such as the cyclobutane derivatives obtained by solid-state [2 + 2] photocycloadditions of cinnamates and other highly conjugated alkenes.^{5–14} Nonetheless, the distance criterion of the topochemical postulate (C...C contacts ≤ 4.2 Å), first established by Schmidt and co-workers,^{5,6} appears to hold well for radical chain reactions in the solid state.^{1–4} ⁶⁰Co γ -ray initiated radical chain solid-state polymerization of solid metal acrylates was first discovered nearly 60 years ago.^{15,16} Ionizing radiation also effectively initiates single-crystal-to-single-crystal solid-state polymerization of a wide range of diacetylenes and muconate esters.^{17–22} Although ⁶⁰Co γ -ray irradiation of solid metal complexes of acrylates, methacrylates, propynoates, and other unsaturated carboxylates showed widespread reactivity,^{15,23} the

polymeric products were mostly amorphous and atactic, with a unique stereoregular example.²⁴

Naruchi and co-workers found that heating crystalline sodium *trans*-2-butenate (**1**) at 300–320 °C stereo- and chemo-selectively provides the dimer disodium *rel*-(3*S*,4*R*)-1-hexene-3,4-dicarboxylate (**2a**) in 84% yield, probably by a thermal ene reaction (see Scheme 1).^{25,26} This facile process suggests that crystalline **1** contains short C...C contacts and a favorable

Scheme 1. Thermal Dimerization of **1** to Give **2a** and γ -Ray-Induced Trimerization of **1** to Give **3a**



Received: October 26, 2020

Revised: December 1, 2020

Published: December 14, 2020

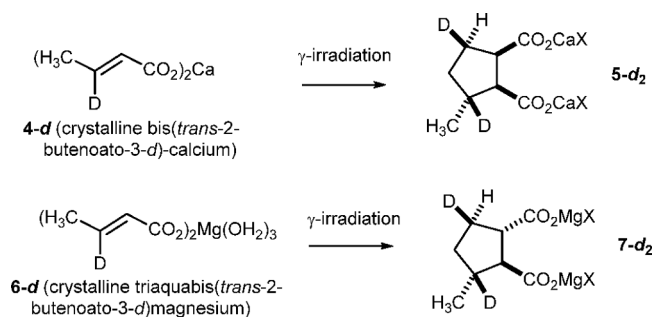


orientation of adjacent molecules that lead to the efficient thermal formation of **2a**. We therefore suspected that **1** might show sensitivity to ionizing radiation and were pleased to find that irradiation of **1** with ^{60}Co γ -rays (156 kGy) initiates a radical chain reaction that affords *one of eight possible diastereomers* of trisodium 2,4-dimethyl-6-heptene-1,3,5-tricarboxylate (**3a**) in 68% yield.¹ The efficient conversion of **1** to **3a** suggested that further exploration of the γ -ray-induced radical chain chemistry of crystalline *trans*-2-butenates would be productive.

Thus, our approach to discovering and elucidating reactive phases was guided by five ideas and/or observations. First, the elegant suggestion by Herbert Morawetz that changing the metal counterion of a reactive unsaturated carboxylate will change the crystal structure, and therefore, the reactivity, provides an efficient way to generate novel crystal structures that may react differently.¹⁵ Second, metal salts and complexes with relatively short radii and coordination numbers of six or less have structural features that might allow short intermolecular contacts and thus would be reactive in the solid state. Third, a survey of the Cambridge Structural Database in 2000 showed that bilayer structures are dominant (92%) for salts and complexes of ≥ 4 -carbon aliphatic acids.^{27,28} Such bilayer structures promote close-packing of the organic side chains, often leading to solid-state reactivity between adjacent groups. Depending upon the structure of a given material and the observed short contacts, reactivity may occur either solely between molecules within one section (i.e., one-half) of a bilayer,^{3,23} or between molecules in the two sections of a bilayer.⁴ Fourth, with a view to exploring solid-state reactivity of the *trans*-2-butenate moiety, we found 147 structures of metal salts and complexes in the current version of the Cambridge Structural Database containing the *trans*-2-butenate anion, including our own contributions.²⁹ We have surveyed many of these, and most do not contain arrangements suitable for γ -ray-induced reactivity. The lack of reactivity is obvious for some, e.g., the high-coordination number complexes of large rare-earth metals in which bulkiness disfavors close approach of unsaturated groups,^{30,31} and complexes containing large ligands that prevent close approach of the butenates³² for alignment of the unsaturated groups. Finally, we note that ammonium *trans*-2-butenate has a bilayer structure and favorable contacts for reaction but is insensitive to γ -rays, suggesting that the presence of a metal is important for *trans*-butenate reactivity.³³ We thus began our study with *trans*-2-butenate salts and complexes of metals with small radii, possible bilayer structures, and no additional ligands other than water.

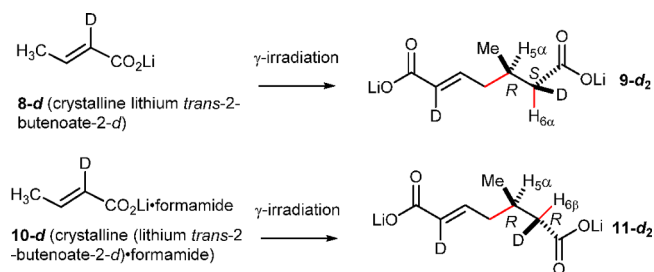
To our delight, irradiation of bis(*trans*-2-butenato)calcium (**4**) with ^{60}Co γ -rays initiates a radical chain reaction that proceeds stereospecifically to give calcium *cis,trans*-nepetate (**5**) as only one of four possible stereoisomers in high yield, but at low conversion (see Scheme 2).^{2,3} The disordered crystal structure of **4** indicates that only 4.8% of the *trans*-2-butenates have the appropriate orientation for the production of *cis,trans*-nepetate **5**. Heating the sample to 60 °C for 24 h between two irradiations of 7 kGy likely induces a “pedal” rotation^{34,35} and increases the yield of **5** to 7.5%. We thought that a group IIA metal with a shorter radius might also form a *trans*-2-butenate salt with the correct orientation to form a cyclodimer, hopefully the diastereomeric *trans,trans*-nepetate **7**. The crystal structure of triaquabis(*trans*-2-butenato)magnesium (**6**) is indeed correctly oriented with short C...C contact distances, and ^{60}Co γ -irradiation of **6** affords *trans,trans*-nepetate (**7**) in high yield at low conversion.³

Scheme 2. Formation of *cis,trans*-Nepetate **5-d₂** and *trans,trans*-Nepetate **7-d₂** by γ -Irradiation of **4-d** and **6-d**, Respectively



In attempting to prepare lithium *trans*-2-butenate, we isolated anhydrous lithium *trans*-2-butenate (**8**) and a solvate, lithium *trans*-2-butenate·formamide (**10**), that both afford the same dimer, dilithium *trans*-5-methyl-2-heptenedioate, upon ^{60}Co γ -irradiation (see Scheme 3).⁴ However, stereochemical

Scheme 3. Formation of Dilithium *trans*-5-Methyl-2-heptenedioates **9-d₂** and **11-d₂** by γ -Irradiation of **8-d** and **10-d**, Respectively



analysis of products **9-d₂** and **11-d₂** from the analogous crystals of **8-d** and **10-d** established that both C–C and C–H bond formation occur stereospecifically by *syn*-addition to the double bond with **8-d** leading to **9-d₂** and by *anti*-addition to the double bond with **10-d** leading to **11-d₂**.⁴

The formation of **3**, **5**, **7**, **9**, and **11** probably proceeds by a radical chain reaction initiated by a γ -ray-induced abstraction of a hydrogen atom from the methyl group to give an allylic radical that then adds to a second molecule of *trans*-2-butenate with an orientation and regiochemistry determined by crystal packing. The crystal lattice controls the two or three propagation steps that produce the observed product and regenerate the allylic radical. Using deuterium-labeled substrates, we established that, in the final propagation step, hydrogen atom transfer is also stereospecific. Although all of these steps individually are preceded in solution, their occurrence to give the observed products selectively is clearly a result of a favorable orientation of the *trans*-2-butenate species in the crystal. The formation of both carbon–carbon bonds and hydrogen atom transfer is unequivocally topochemical, stereospecific, and not the result of a random process.^{3,4} As indicated above, γ -ray-initiated solid-state polymerization reactions have been extensively studied.^{15–24} On the other hand, there are very few examples of reactions of radical chain solid-state reactions that lead *cleanly* to monomeric, dimeric, or trimeric compounds. In addition to the formation of **3**, **5**, **7**, **9**, and **11**, the only examples we are aware of are the isomerizations of α -lactose monohydrate,^{36,37} D-fructose,^{36,38–40} and 2-deoxy- β -D-erythro-pentopyra-

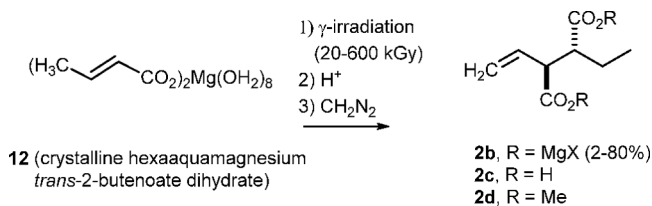
nose^{36,41} and the dimerization of a bis alkyne.⁴² In all of the highly stereospecific reactions we studied, the single crystals become amorphous as the reaction proceeds. While there are many examples of single-crystal-to-single-crystal transformations that arise from thermal and/or photochemical processes,^{43,44} we are unaware of examples of γ -ray-induced transformations that proceed to monomeric, dimeric, or trimeric compounds with retention of single-crystal quality.

The γ -ray-induced radical chain solid-state dimerization reactions of *trans*-2-butenic acid are orthogonal to the better-known solid-state [2 + 2] photocycloadditions of cinnamates and other highly conjugated alkenes.^{5–14} Cinnamates lack the allylic hydrogen atom needed for initiation of the radical chain upon γ -irradiation. Even with the heavy atom, crystalline (*E*)-4-bromocinnamic acid affords the cyclobutane dimer β -truxinic acid in only 24% yield after exposure to a very large 1160 kGy γ -ray dose.⁴⁵ Similarly, γ -irradiation (30–5000 kGy) of crystalline *trans,trans*-2,4-hexadiendioic acid, its methyl ester, or *trans,trans*-2,4-hexadienoic acid provides only \sim 2% dimer and no oligomer, whereas ultraviolet irradiation produces the cyclobutane dimers in 60% yield.^{46,47} It was proposed that photochemical dimerization involves direct reaction between an excited double bond and an adjacent double bond in the ground state, while γ -irradiation produces highly excited states that break down without giving the particular state necessary for dimerization.⁴⁶ Conversely, the allylic hydrogen atoms, which are needed for γ -ray-induced free-radical chain dimerizations and trimerizations of *trans*-2-butenates, prevent [2 + 2] photocycloaddition on UV irradiation. *trans*-2-Butenoic acid isomerizes to *cis*-2-butenic acid, which then undergoes photoenolization by 1,5-sigmatropic hydrogen shift and protonation to give 3-butenic acid.^{48,49}

RESULTS AND DISCUSSION

Solid-State Chemistry of 12. Slow evaporation of aqueous solutions of magnesium *trans*-2-butenate over 1–2 weeks gave two different types of crystals, prismatic hexaaquamagnesium *trans*-2-butenate dihydrate (12) and plate-like triaquabis-(*trans*-2-butenato)magnesium (6), which could be separated manually (see Scheme 4). Alternatively, a diffusion technique

Scheme 4. Conversion of 12 to *rel*-(3*S*,4*R*)-1-Hexene-3,4-dicarboxylate (2b) by γ -Irradiation



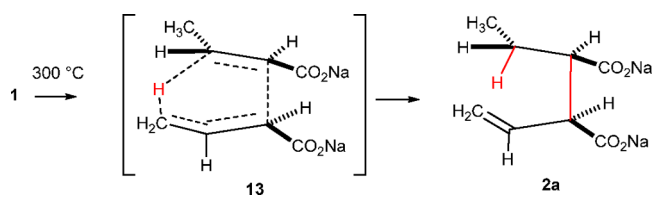
could be used by layering 5–10 volumes of an organic solvent on top of the aqueous solution. This was selective for the crystallization of 12 with several organic solvents and for the crystallization of 6 with DMF.³ We have previously reported the γ -ray-initiated reactions and structural chemistry of 6 to give 7.³ The γ -ray-initiated reactions and the results of an extensive study of the structural chemistry of single crystals of 12 are described below.

Samples of 12 were irradiated in capped vials under air for 2–128 d at 5 kGy/day. The samples were dissolved in D_2O and analyzed by ^1H NMR spectroscopy, which showed increased

conversion of 12 to 2b over time: 2 d (0%), 4 d (1.8%), 8 d (7.4%), 16 d (23.1%), 32 d (45.5%), 64 d (65.6%), and 128 d (80.3%). The ^1H NMR spectrum of 2b was identical to that of authentic 2a prepared by heating 1 at 300 °C as reported by Naruchi.²⁵ The NMR spectrum of a mixture of sodium salt 2a and magnesium salt 2b showed that only a single organic moiety was present. Thus, the dimerization of 12 to form 2b is a *sixth* mode of γ -ray-initiated radical chain chemistry of *trans*-2-butenate that once again occurs under topochemical control.^{1–4}

The formation of 2 by both the pyrolysis of 1 and the γ -ray-initiated radical chain reaction of 12 was surprising. The conversion of 1 to 2a most likely occurs by a thermal ene reaction as shown in Scheme 5. Like the better-known Diels–

Scheme 5. Thermal Concerted Ene Reaction of 1 to Give 2a



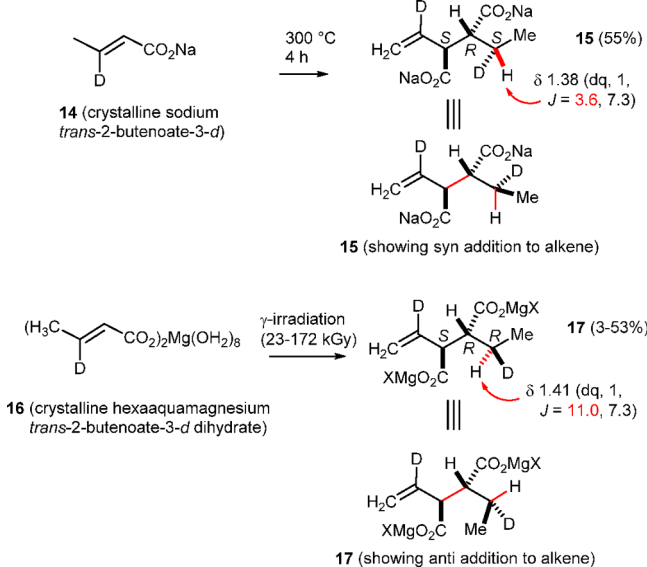
Alder reaction, the ene reaction is a concerted reaction proceeding through transition state 13 that typically occurs on heating. However, an ene reaction of 12 to give 2b cannot occur at room temperature by γ -irradiation. Dimer 2b must be formed by a different mechanism.

As we have previously reported,^{3,4} deuterium labeling provides important stereochemical information about the mechanism of formation of 5, 7, 9, and 11, and we thought it would also be helpful in understanding the mechanism of formation of 2a and 2b. *trans*-2-Butenoic-3-*d* acid was prepared as we have previously described³ and converted to crystalline sodium *trans*-2-butenate-3-*d* (14) and crystalline hexaaquamagnesium *trans*-2-butenate-3-*d* dihydrate (16) analogously to the preparation of 1 and 12 (see Scheme 6).

A sample of 14 sealed under vacuum was heated for 4 h at 300 °C to give 55% of disodium *rel*-(3*S*,4*R*,5*S*)-1-hexene-3,4-dicarboxylate-2,5-*d*₂ (15) and 45% of unreacted 14. A sample of 16 sealed under vacuum was γ -irradiated to give a mixture of unreacted 16 and magnesium *rel*-(3*S*,4*R*,5*R*)-1-hexene-3,4-dicarboxylate-2,5-*d*₂ (17). The conversion was about 3% after 12 d, 28% after 30 d, and 53% after 90 d. Most significantly, the geminal coupling constant between H_4 and H_5 of 15 is 3.6 Hz, whereas that of 17 is 11 Hz. This unambiguously establishes that the addition to the double bond is *syn* for 15 and *anti* for 17, as discussed below.

Conformational analysis^{50–56} suggests that the C_4 – C_5 bond preferentially adopts the conformation shown with the methyl group on C_5 *anti* to the large $\text{CH}_2=\text{CH}(\text{CO}_2\text{H})\text{CH}$ substituent on C_4 as shown in the top structures in Scheme 6. This allows the assignment of structure 15 to the product from 14 because the dihedral angle between H_4 and H_5 is 60°, resulting in a small 3.6 Hz coupling constant and assignment of structure 17 to the product from 16 because the dihedral angle between H_4 and H_5 is 180°, resulting in a large 11.0 Hz coupling constant. Examination of the red bonds in the lower structures of Scheme 6 indicates that the addition to the double bond of 14 is *syn* as expected for the thermal ene reaction shown in Scheme 5, whereas the addition to the double bond of 16 is *anti*, as

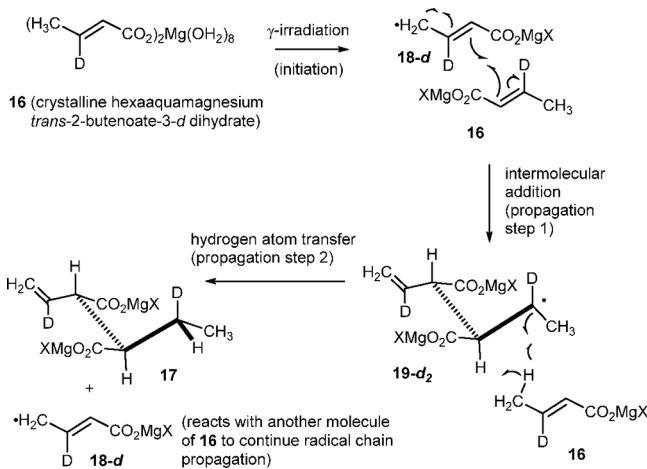
Scheme 6. Thermal Dimerization of 14 to Give *rel*-(3*S*,4*R*,5*S*)-1-Hexene-3,4-dicarboxylate-2,5-*d*₂ (15) and γ -Ray-Initiated Dimerization of 16 to Give *rel*-(3*S*,4*R*,5*R*)-1-Hexene-3,4-dicarboxylate-2,5-*d*₂ (17)



expected for an intermolecular hydrogen atom transfer in a radical chain reaction.

A plausible mechanism for the formation of **17** (bisdeuterated **2b**) is shown in Scheme 7. γ -Ray initiation by abstraction of a

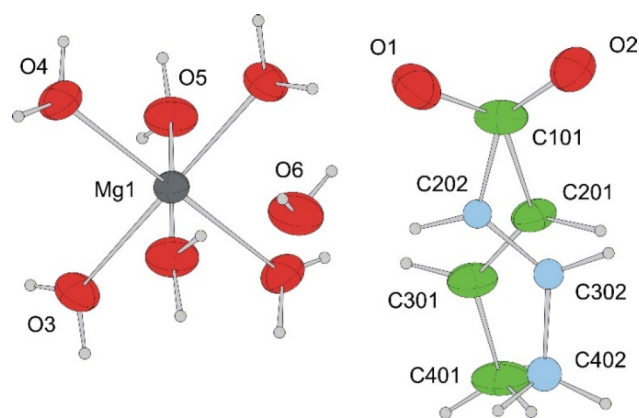
Scheme 7. Radical Chain Mechanism for the Conversion of 16 to 17



hydrogen atom of **16** gives allylic radical **18-d**, which adds to a second molecule of **16** in the first propagation step to give dimeric radical **19-d₂**. The regio- and stereochemistry of the addition are controlled topochemically. In the second propagation step, a third molecule of **16** transfers a hydrogen atom to the radical **19-d₂** to generate the product **17**, and a second molecule of allylic radical **18-d** that continues the chain. Because this hydrogen atom transfer is intermolecular and the molecular motion of **19-d₂** is restricted by the crystal lattice, the addition to the double bond should be stereospecifically *anti* as is observed.

Structural Chemistry of Hexaaquamagnesium *trans*-2-Butenoate Dihydrate. Single crystals of **12** were grown by

diffusion of a layered acetone–magnesium *trans*-2-butenate aqueous solution; details may be found in the Experimental Section. An X-ray structure determination of **12** prior to exposure to ⁶⁰Co γ -rays showed it to crystallize in the triclinic system, space group *P*1̄, with *Z* = 1. The asymmetric unit, which consists of one-half of a hexaaquamagnesium dication, one molecule of water of hydration, and a disordered *trans*-2-butenate anion, is shown in Figure 1. The magnesium ion



occupies a center of symmetry; Figure 1 shows the full six-coordinate cation for completeness. The anion disorder was refined with the constraint that the two fractional occupancies of the anion (0.684(4)/0.316(4)) sum to 1.0. Only the disordered CH₃CH=CH– portions of the anion could be resolved. Figure 1 shows the numbering scheme for the major component atoms (C201, C301, and C401 in green) and minor component atoms (C202, C302, and C402 in blue) that could be resolved. Summary experimental details of the structure determination appear in Table 1A; full details are available in the Supporting Information. Unlike many salts and complexes of metals with *trans*-2-butenate, the metal in compound **12** is not bonded to the oxygen atoms of the *trans*-2-butenate anion. As shown in the packing diagram (Figure 2), the *trans*-2-butenate anions reside in a cavity in the center of the unit cell along with two water molecules of hydration and hexaaquamagnesium cations at the eight unit cell corners. In discussion of the important contacts for all of the structural chemistry in this paper, we will use the atomic numbering system in the figures, defining the contact's symmetry-related position once, and always designating the symmetry-related atom by a prime-symbol. Thus, here the dashed line shows a contact distance of 3.792(3) Å between atom C201 and symmetry-related atom C201' ($-x, -1-y, -1-z$). The facile γ -ray-induced dimerization process, by which **12** is converted to **2b** in the solid state, is consistent with the hypothesis that crystalline **12** contains short C⋯C contacts and that topochemical effects, *viz.*, C⋯C contacts less than 4.2 Å (3.792(3) Å in the major component and 3.451(6) Å in the minor component) and a favorable orientation of adjacent molecules for reaction, are responsible for both the efficiency of

Table 1A. Crystallographic Data for Crystal 1^a

crystal codes	0_1	8_1	16_1	32_1
<i>a</i> (Å)	7.6047(3)	7.5950(2)	7.5729(4)	7.5673(3)
<i>b</i> (Å)	7.8363(3)	7.8383(2)	7.8451(5)	7.8510(3)
<i>c</i> (Å)	7.8674(4)	7.8615(3)	7.8437(3)	7.8306(3)
α (deg)	106.515(4)	105.902(2)	104.505(4)	103.826(3)
β (deg)	100.002(4)	99.993(2)	100.024(4)	100.118(3)
γ (deg)	104.777(3)	105.158(2)	105.945(5)	106.216(3)
<i>V</i> (Å ³)	419.02(4)	419.01(2)	418.76(4)	418.85(3)
<i>Z</i> , <i>Z'</i>	1, 0.5	1, 0.5	1, 0.5	1, 0.5
F.W., g mol ⁻¹	169.3	169.3	169.3	169.3
space group	<i>P</i> $\bar{1}$	<i>P</i> $\bar{1}$	<i>P</i> $\bar{1}$	<i>P</i> $\bar{1}$
<i>T</i> (K)	294	294	294	294
λ (Å)	0.71073	0.71073	0.71073	0.71073
ρ_{calc} (g cm ⁻³)	1.342	1.342	1.342	1.342
μ (mm ⁻¹)	0.158	0.158	0.158	0.158
θ_{max} ; trans. factors	30.4°; 0.87–0.91	30.4°; 0.88–0.91	30.4°; 0.88–0.91	30.4°; 0.88–0.91
<i>R</i> , <i>R_w</i> (<i>I</i> > 2 σ (<i>I</i>))	0.0368, 0.0445	0.0475, 0.0599	0.0472, 0.0575	0.0481, 0.0606
<i>R</i> , <i>R_w</i> (all data)	0.0465, 0.0593	0.0593, 0.0784	0.0603, 0.0780	0.0607, 0.0800
<i>S</i>	1.042	1.046	1.020	1.035
no. refl. (<i>I</i> > 2 σ (<i>I</i>); all)	2112; 2530	2047; 2529	2018; 2527	2037; 2526
no. param.	143	153	152	152
major/minor reactant; ratio	0.684(4)/0.316(4) 2.165	0.592(4)/0.273(2) 2.165	0.387(4)/0.179(2) 2.162	0.266(4)/0.123(2) 2.162
major/minor product; ratio		0.092(4)/0.043(2) 2.160	0.297(4)/0.137(2) 2.168	0.418(4)/0.193(2) 2.165
extent of reaction	0	0.135(6)	0.434(6)	0.611(6)

$$^a R = \sum ||F_o| - |F_c|| / \sum |F_o|; R_w = [\sum w(|F_o| - |F_c|)^2 / \sum w(F_o)^2]^{1/2}; S = [\sum w(|F_o| - |F_c|)^2 / (n - m)]^{1/2}$$

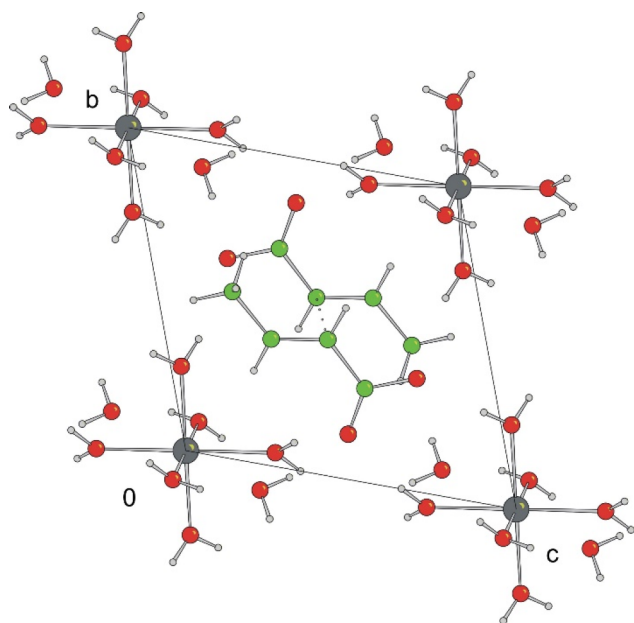


Figure 2. View of the crystal structure of **12** viewed down the crystallographic *a* axis. Only the major components of the disordered *trans*-2-butenate are shown, with a contact distance of 3.792(3) Å between α -carbon atoms C201 and C201' (see text). The minor component of the disorder (see Figure S1) has an α -carbon contact distance of 3.451(6) Å between atom C202 and symmetry-related atom C202' ($-x, -1-y, -1-z$).

the process as well as the stereochemistry of the product as discussed in detail below.

The disorder of the *trans*-2-butenate groups is a consequence of a “relatively spacious” cavity, with only the oxygen atom end of the *trans*-2-butenates held securely by strong hydrogen bonds. The lack of restrictive contacts is expected to facilitate the

molecular motion that must occur during the solid-state dimerization process. There are eight strong hydrogen bonds in the structure, involving all six coordinated water molecules as well as the two molecules of hydrated water, with O...O contact distances ranging from 2.74 to 2.85 Å and O–H...O angles ranging from 160° to 174°; the full listing appears in Table S1. Most of the hydrogen bonds are shown in Figure 3.

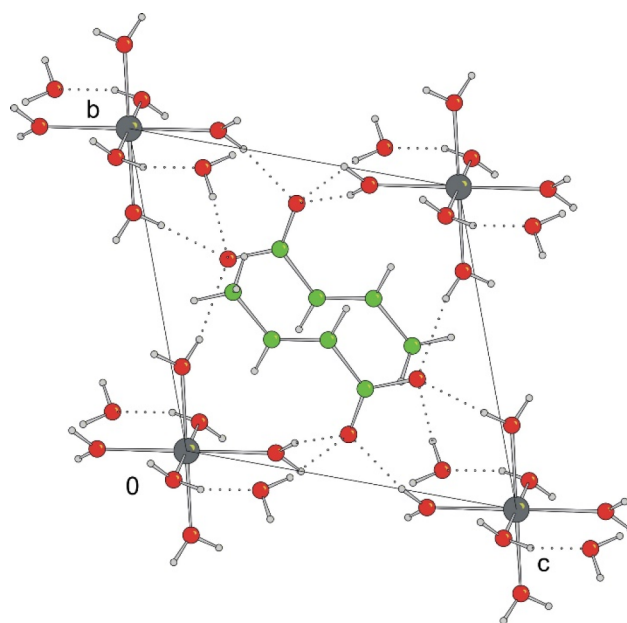


Figure 3. View of the hydrogen bonds in the crystal structure of **12**, viewed down the crystallographic *a* axis. Only the major components of the disordered *trans*-2-butenate are shown. All hydrogen bonds are shown at least once except for the coordinated water-to-solvate water hydrogen bond, O5–H81...O6.

Single-Crystal-to-Single-Crystal Solid-State Reaction of 12 to Give 2b.

Past experience suggested that the crystals would likely become amorphous as the reaction proceeded to convert 12 to 2b in the solid state.^{1–4,15,16,23,24} After ⁶⁰Co γ -irradiation of X-ray quality crystals, an exploratory X-ray structure determination of a partially reacted crystal revealed the presence of product in the area of the *trans*-2-butenate anions. Thus, we concluded that the cavity created by the eight hexaaquamagnesium cations had sufficient free space to allow reaction to occur without significant disruption of the crystal. Crystals of 12 were beautifully faceted and clear at the outset and did not degrade optically upon irradiation. Therefore, we decided to study the extent of the solid-state reaction versus irradiation dose, hopefully in a set of three or four single crystals that would survive the required months of γ -irradiation. The composition of the material, with eight water molecules per unit cell, was a concern over an extended period of irradiation, with previously observed dehydration-cum-loss of crystal quality. The six crystals were coated with perfluoropolyether, placed into glass capillaries, and affixed to the capillary walls with epoxy; the capillaries were sealed using a hot wire. At the time of this experimental work, a CCD machine was not available in our laboratory, nor was a low-temperature device. (The latter restriction was good fortune, as we later discovered that compound 12 undergoes an enantiotropic, polymorphic phase transition to a different cell at *ca.* 274 K.⁵⁷) High-quality, high-resolution data were collected at RT on an Enraf-Nonius CAD-4 Turbo diffractometer equipped with Mo K α radiation. After data collection, crystals were irradiated for various times with ⁶⁰Co γ -rays at Brandeis University (Gammacell 220 Irradiator, Atomic Energy of Canada, Ltd., dose rate 2.6 kGy/day). The crystals were periodically removed from the γ -ray irradiator, and their structures were redetermined. The process was repeated until the crystals reached maximum conversion (*ca.* 5 cycles). Two crystals degraded to an unidentified polycrystalline material, owing to water loss after one or two cycles, and further studies of those two samples were abandoned. For the four crystals studied, irradiation was carried out for 8, 16, 32, 56, and 110 days (20.8, 41.6, 83.2, 145.6, and 286 kGy, respectively). In order to establish either completeness or plateauing of conversion after the initial 286 kGy at Brandeis University, crystals 1 and 2 were irradiated with an additional 650 kGy γ -ray dose at the Radiation Laboratory, University of Massachusetts, Lowell (dose rate of 20 kGy/h).

The summary of experimental details appears in Tables 1A and 1B for crystal 1. The reaction takes place in a single crystal, with no change in space group, and the unit cell constants change gradually by small amounts. No new diffraction pattern appears, and thus, the solid-state reaction takes place within a single phase. In Tables 1A and 1B, each crystal is denoted by a code **n1_n2**, where **n1** is the number of exposure days, and **n2** is the crystal number. Thus, entry 32_1 is the column for data collection on crystal 1 after 32 days (83.2 kGy exposure); for crystals 1 and 2, which received an additional 650 kGy dose, the codes are 110_65m_1 and 110_65m_2. In the Supporting Information, the six Tables S2_0 through S2_110 each contain all of the information presented in Tables 1A and 1B, with each row given for each irradiation time of crystals 1–4, and Table S2_110_65m presents the analogous data for the extra radiation dose received by crystals 1 and 2. Inspection of all the tables reveals a remarkable consistency in the crystallographic results for the four crystals over a period of nearly four months (110 kGy γ -ray dose, plus the additional dose of 650 kGy for crystals 1

Table 1B. Crystallographic Data for Crystal 1^a

crystal codes	56_1	110_1	110_65m_1
<i>a</i> (Å)	7.5639(3)	7.5620(3)	7.5303(3)
<i>b</i> (Å)	7.8542(4)	7.8564(3)	7.8573(3)
<i>c</i> (Å)	7.8221(2)	7.8178(4)	7.8219(3)
α (deg)	103.461(3)	103.227(4)	103.049(3)
β (deg)	100.176(3)	100.216(4)	100.170(3)
γ (deg)	106.330(4)	106.380(3)	106.545(4)
<i>V</i> (Å ³)	418.85(3)	418.98(3)	417.56(3)
<i>Z</i> , <i>Z'</i>	1, 0.5	1, 0.5	1, 0.5
F.W., g mol ⁻¹	169.3	169.3	169.3
space group	<i>P</i> $\bar{1}$	<i>P</i> $\bar{1}$	<i>P</i> $\bar{1}$
<i>T</i> (K)	294	294	294
λ (Å)	0.71073	0.71073	0.71073
ρ_{calc} (g cm ⁻³)	1.342	1.342	1.346
μ (mm ⁻¹)	0.158	0.158	0.159
θ_{max} ; trans. factors	30.4°; 0.88–0.91	30.4°; 0.90–0.91	30.4°; 0.90–0.91
<i>R</i> , <i>R_w</i> (<i>I</i> > 2 σ (<i>I</i>))	0.0472, 0.0633	0.0489, 0.0689	0.0489, 0.0629
<i>R</i> , <i>R_w</i> (all data)	0.0582, 0.0833	0.0612, 0.0934	0.0662, 0.0978
<i>S</i>	1.003	0.970	0.965
no. refl. (<i>I</i> > 2 σ (<i>I</i>); all)	2081, 2528	2058, 2528	1936, 2520
no. param.	152	152	152
major/minor reactant; ratio	0.184(4)/0.085(2) 2.165	0.134(5)/0.062(2) 2.161	0.157(7)/0.073(3) 2.151
major/minor product; ratio	0.500(4)/0.237(2) 2.110	0.550(5)/0.254(2) 2.165	0.527(7)/0.243(3) 2.169
	2.110	2.165	2.169
extent of reaction	0.731(6)	0.805(7)	0.770(11)

^a $R = \sum ||F_o| - |F_c|| / \sum |F_o|$; $R_w = [\sum w(|F_o| - |F_c|)^2 / \sum w|F_o|^2]^{1/2}$; $S = [\sum w(|F_o| - |F_c|)^2 / (n - m)]^{1/2}$

and 2). Below we first consider the structural chemistry of reactant and product and then examine the consistency of the single-crystal-to-single-crystal reactions throughout the four-crystal experiment.

Panels a and b of Figure 4 show the major and minor components of the disordered *trans*-2-butenate anions, respectively, as observed in the structure of 12 prior to irradiation. The pairs of molecules are related by a center of symmetry and are chosen to show the shortest α -carbon to α -carbon contacts for each component. Both distances are well within the 4.2 Å limit of the Schmidt topochemical postulate for photochemical reactions, which we and others have shown also to be a highly useful criterion for radiation-induced radical reactions in the solid state.^{2–4,16–24} The short distance, and the centrosymmetric orientation of the reactants in each case, would be expected to lead to the observed topochemical product, magnesium *rel*-(3*S*,4*R*)-1-hexene-3,4-dicarboxylate (2b).

After the initial irradiation period, the structure of the mixed reactant/product crystals could be solved by conventional means. The structure, presented in Figures 5 and 6, involves a complex four-component disorder, because each disordered reactant component yields a different product orientation, and as can be seen in Tables 1A and 1B, the reaction does not proceed to completion. Figures 5b and 6b show the numbering scheme for the resolvable product major component atoms (C2, C3, and C4) and the product minor component atoms (C21, C31, and C41), respectively.

Thus, for example, at maximum conversion, the crystal contains 20% of the two original monomer components and 80% of the two resultant product components. The successful refinement required a thoughtful analysis and consideration of a

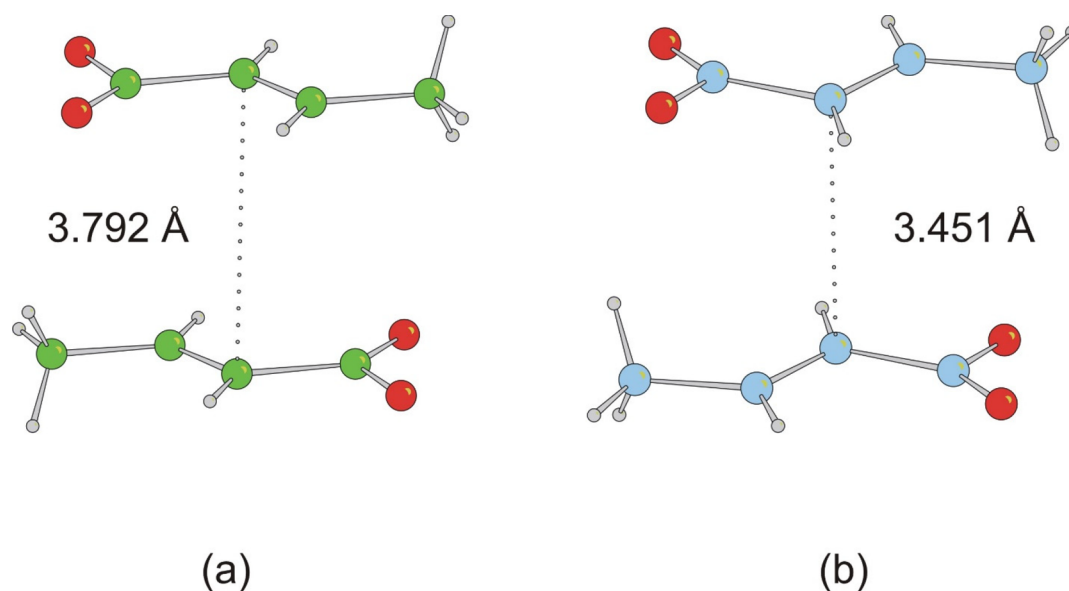


Figure 4. (a) View of a pair of major-component reactant molecules related by an inversion center and appropriately oriented to form **2b**, a *rel*-(3*S*,4*R*)-1-hexene-3,4-dicarboxylate moiety; (b) the analogous view for the minor component reactant pair.

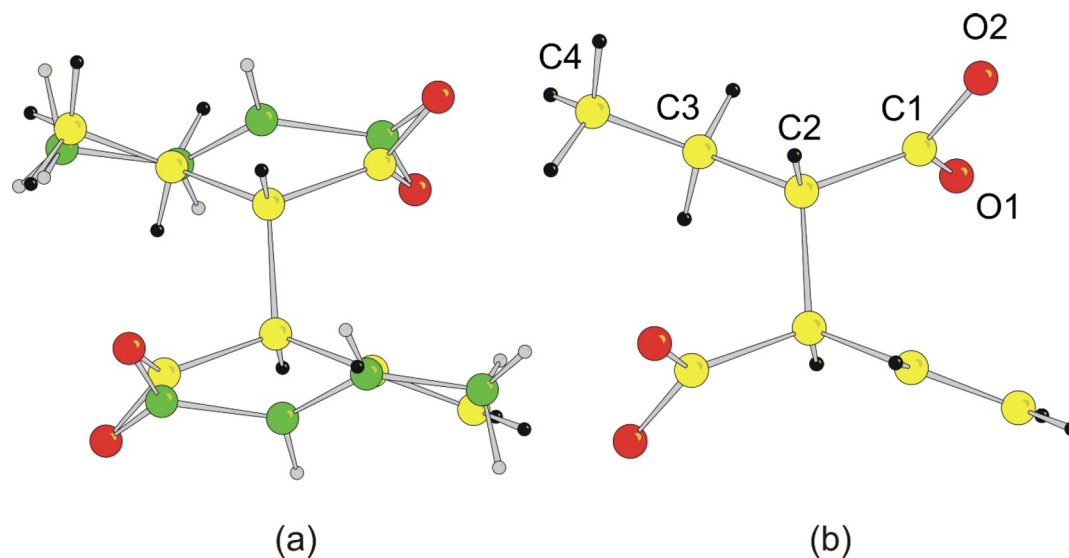


Figure 5. (a) View of a pair of inversion-related, major-component reactant molecules of **12** superimposed on the major product component, *rel*-(3*S*,4*R*)-1-hexene-3,4-dicarboxylate **2b**; (b) the identical view with the reactant molecules removed. Reactants have green C atoms and gray H atoms, while product molecules have yellow C atoms and black H atoms. Disorder of the product molecule is not shown, and disorder of the O atoms was not resolved (view from 32-day irradiation). The bond distance between the α -carbon atoms C2 and C2' ($-x, -1-y, -1-z$) is 1.558(6) Å.

proper set of constraints and restraints. Many different combinations of restraints were attempted, but in the end, three general restraints helped ensure a stable and consistent refinement of all 26 determinations. The conditions applied were as follows: (i) the occupancies of reactant and product were restrained to sum to 1.0; (ii) the ratio of major/minor product occupancies and the ratio of major/minor reactant occupancies were restrained to be equal by restraining their difference to be 0.0; and (iii) for carboxylate carbon atom C1 of the product, where disorder could not be resolved, the occupancy of C1 and the sum of the occupancies of the major and minor product were restrained to be equal by restraining the difference to be 0.0. An analogous restraint was applied to the occupancy of reactant carboxylate carbon atom C101. The equations used may be found in the deposited CIF files. In

simpler language, disorder of C1 and C101 could not be resolved, so that (a) the occupancy of C1 is the sum of the occupancies of the two components of product and (b) the occupancy of C101 is the sum of the occupancies of the two components of reactant.

The X-ray structure determination of the solid solution of **12** and **2b** confirms the stereochemistry of **2b** assigned by Naruchi²⁵ by hydrogenation of acid **2c** to give *meso*-2,3-diethylsuccinic acid, mp 192 °C (lit.⁵⁸ 187–206 °C), rather than (\pm)-2,3-diethylsuccinic acid, mp 130–134 °C.⁵⁸ We have the rare opportunity to confirm the structure of product **2b** by analysis of the X-ray data without purification and crystallization of the product. In our previous work^{1–4} with *trans*-2-butenates, the crystals became amorphous upon irradiation.

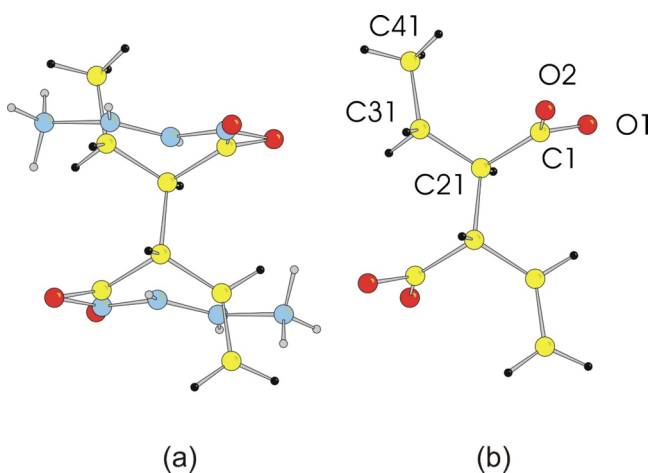


Figure 6. (a) View of a pair of inversion-related, minor-component reactant molecules of **12** superimposed on the minor product component *rel*-(3*S*,4*R*)-1-hexene-3,4-dicarboxylate **2b**; (b) the identical view with the reactant molecules removed. Reactants have blue C atoms and gray H atoms, while product molecules have yellow C atoms and black H atoms. Disorder of the product molecule is not shown, and disorder of the O atoms was not resolved (view from 32-day irradiation). The bond distance between α -carbon atoms C21 and C21' ($-x, -1-y, -1-z$) is 1.529(13) Å.

Figure 5a shows the superposition of major component reactant and product, while Figure 6a shows the analogous view for minor component reactant and product. The complete structure is a superposition of Figures 5a and 6a. The reader is encouraged to view these two figures as PowerPoint animations in the Supporting Information file Figures 5 and 6.pptx. It is notable that the reacting C atom distance is longer for the major component (Figure 4), but the amount of molecular motion is greater for the minor component. Figures 5b and 6b show a “partial” (i.e., undistorted) structure of the dimeric product, *rel*-(3*S*,4*R*)-1-hexene-3,4-dicarboxylate. The dimer occupies a center of symmetry, which results in a 1:1 disorder of the CH₂=CH– and CH₃CH₂– ends of the molecule. The torsion angles C1–C2–C2'–C3' and C4–C3–C2–C2' for the major product are 60.5(11)° and 98.5(14)°, while torsion angles C1–C21–C21'–C31' and C41–C31–C21–C21' for the minor product are –54.6(11)° and 175.9(11)°, respectively. While there are only a few structural analogues for the 98.5° and 175.9° torsion angles, the two different values appear to represent the expected values for each “end” of the disordered product. The major isomer is near to values observed for unsaturated analogues²⁹ LISVUG (124°),⁵⁹ LISWAN (–129°),⁵⁹ and LISWIV (–122°),⁵⁹ while the minor isomer value is in good agreement with the saturated analogues JOKJOI (177°),⁶⁰ KAGJUX (161°),⁶¹ and VODFOJ (–174°).⁶²

Examination of Tables 1A and 1B reveals some interesting observations. First, the ratios of reactant and product disorder versus total dose are equal within experimental error; a conservative estimate of the standard uncertainties of the ratios sets the range of values to 0.02–0.07 (see also Tables S2_0 through S2_110 for the entire crystal set). All values are within ± 3 standard uncertainties. Second, the extent of conversion begins to plateau between 32 and 110 days of irradiation, reaching a maximum value of *ca.* 80% after 110 days (286 kGy). A further 650 kGy dose does not increase the amount of product. It appears that, after 110 days of irradiation, further exposure only contributes to radiation damage (see also Table

S2_110_65m). Third, inspection of Tables S2_0 through S2_110 for crystals 1–4 shows that there is a smooth change in all cell constants versus irradiation and no evidence for a phase transition. The cell data for crystals 1–4 are remarkably similar in each table, along with the extent of conversion versus dose, which demonstrates the reproducibility of these experiments. Fourth, we note that the conversion rate of the single crystals of **12** sealed in capillaries is approximately twice as fast as that of powdered **12** under air in vials, although both plateau at 80% conversion. The irradiation time in days is comparable, but the dose rate is 5 kGy/day for powdered **12** and 2.6 kGy/day for the single crystals of **12**, because the latter experiments were conducted five years (i.e., one-half-life) later. Possible reasons for this include shorter chain length resulting from termination of the radical chain by adventitious oxygen in powdered **12**, partial decomposition of powdered **12** by loss of water leading to shorter chain length, and better initial crystal quality of the single crystals. Finally, we note that the smallest unit cell volumes are at the 8–16 day exposure times. However, the maximum differences are very small: for crystals 1–4, they are all less than 0.1%. The values are 0.26(6), 0.27(6), 0.29(5) and 0.39(22) Å³, respectively. Compound **12** differs from the others we have studied in that the reactants are enclosed in a cavity, in which molecular motion is possible, and retention of crystallinity is thus considerably more likely.

As mentioned in the first section, the radiation-induced dimerization of **12** yields only a single diastereomer, the *rel*-(3*S*,4*R*)-1-hexene-3,4-dicarboxylate dianion **2b**. As a topochemical product, the diastereomer can be produced only by a reactant pair consisting of either major/major or minor/minor components. If a “cross-reaction” occurs, i.e., a major/minor pair reacts, as illustrated in Figure 7, the product will be the alternative diastereomer, *rel*-(3*S*,4*S*)-1-hexene-3,4-dicarboxylate. Thus, this is a rare case where “the reaction chemistry

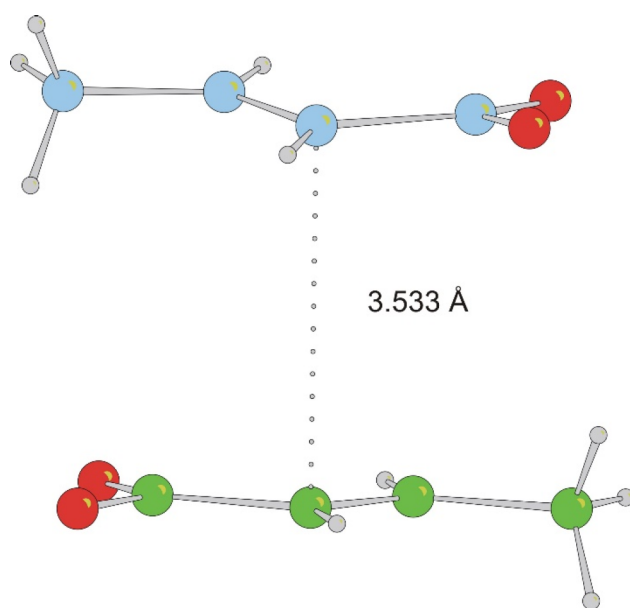


Figure 7. View of a pair of major-component reactant molecule of **12** (below) and a minor-component (above) molecule of **12**, including the α -carbon distance. If such a “cross-reaction” were to occur, the expected topochemical product would be *rel*-(3*S*,4*S*)-1-hexene-3,4-dicarboxylate, which was not observed by NMR analysis or by solution of the crystal structure.

tells us about the crystallography". The overall disorder could involve a 2.165:1 random mixture of carboxylates, above and below the inversion center. However, the chemical result precludes that option as long as the disorder is static. In a separate study, we observed the identical ratio of components in a pristine sample in the temperature range 274–320 K, consistent with static disorder of the molecules.³⁷ The chemistry and the static nature of the disorder are consistent only with inversion-paired reactants.

Structure–Reactivity Relationships for Hydrogen Transfer in 12. In order to develop an understanding of thermal and photochemical solid-state dimerization, we need only to analyze the spatial orientation of *two* molecules of the monomer as depicted in Figure 4. Crystal structure data from the 16-day and 32-day irradiations had reactant/product ratios nearest to 1:1, and the data from the 32-day exposure were used in the calculations and illustrations which follow. The radical chain dimerization depicted in Schemes 6 and 7 involves *three* molecules of monomer and further requires that radical 19 produced in propagation step 2 be appropriately oriented to continue the chain. The deuterium-labeling experiment using 16 provides stereochemical information about the hydrogen atom transfer (propagation step 2). To determine whether hydrogen atom transfer is topochemical, we first consider the relationships for C–C bond formation beginning with each of the two orientations of reactant, as illustrated in Figure 4. We then add an additional *trans*-2-butenoate molecule by symmetry, with the criteria for choice being simply that the added molecule possesses the shortest intermolecular methyl hydrogen to β -carbon atom distance. We then determine whether the predicted stereochemistry of carbon–carbon bond formation and hydrogen atom transfer is consistent with the observed stereochemistry of the deuterium-labeled dimer 16. As stated earlier, the dimerization about a center of symmetry is expected to yield magnesium *rel*-(3*S*,4*R*)-1-hexene-3,4-dicarboxylate, but we now need to establish the topochemical nature of the hydrogen abstraction. The nearest methyl H atom for propagation step 2 is C3...H4012' ($1-x, -1-y, -1-z$) at a distance of 4.521 Å, using a dimer molecule for C3 and a monomer molecule for the hydrogen atom transfer. Monomer–monomer (4.547 Å) and dimer–dimer (4.043 Å) distances are similar, with a somewhat shorter dimer–dimer distance.

The complete relationship for the geometrical course of the reaction is shown in Figure 8. The reader is strongly encouraged to view Figures 8 and 9 as annotated PowerPoint animations in the Supporting Information file [Mechanism.pptx](#). The animation presents the process in a much clearer fashion than can be illustrated in a single figure. Initiation (INIT) occurs with breaking of a C401–H bond and formation of radical 18 (see Scheme 7) at atom C401. Propagation step 1 (label 1) involves bond formation between the α -carbon atoms (green color, just above and below the new bond) of the monomer to form the C2–C2' bond, along with the formation of radical 19 at atom C3. Propagation step 2 (label 2) involves the abstraction of hydrogen atom H4012 from a symmetry-related C401 atom (see above). Another radical 18 is created in step 2, and a second round of propagation begins with the first step (label 3) forming a C2–C2' bond and radical 19 at C3, followed by the second step 2 with abstraction of another H4012 atom from methyl carbon atom C401 (label 4). The third round of propagation begins in a like manner with bond formation and radical 19 generation (step 1, label 5) and the partially shown step 2 (label

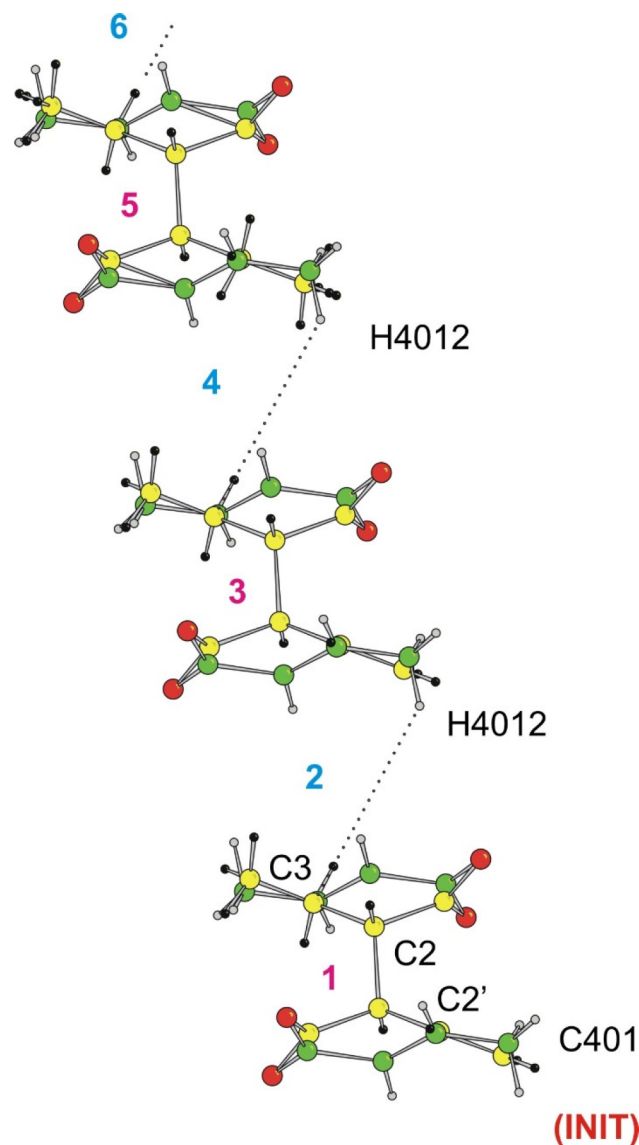


Figure 8. View of the set of superimposed major-component reactant/product molecules shown in Figure 5a, with two additional sets translated by one and two unit cells along the *a* direction, in order to show the likely geometrical mechanism of the radical chain reaction, as described in the text.

6). The torsion angle of approach, C2'–C2–C3...H4012, is excellent for *anti*-addition at 176.3°.

For the minor component reaction, the diagram must be constructed in a different fashion. Examination of a diagram similar to that of Figure 8, but using all minor-component reactants and products, shows an unsatisfactorily short intermolecular γ -carbon to γ -carbon atom C41...C41' ($1-x, -1-y, -1-z$) contact of 2.640 Å for the products. With a major/minor component ratio of *ca.* 2.2:1, the major-component mechanistic reaction pathway (Figure 8) must be considered, but we cannot use the same process to propose a sensible mechanism for the minor component: the single-crystal-to-single-crystal radical chain process cannot proceed under those circumstances. Thus, we hypothesized that, if (a) there were a minor component pair interleaved between two major component pairs and (b) it could be shown that this arrangement did not lead to unusually short contacts, the result would be a consistent geometrical mechanism that includes the

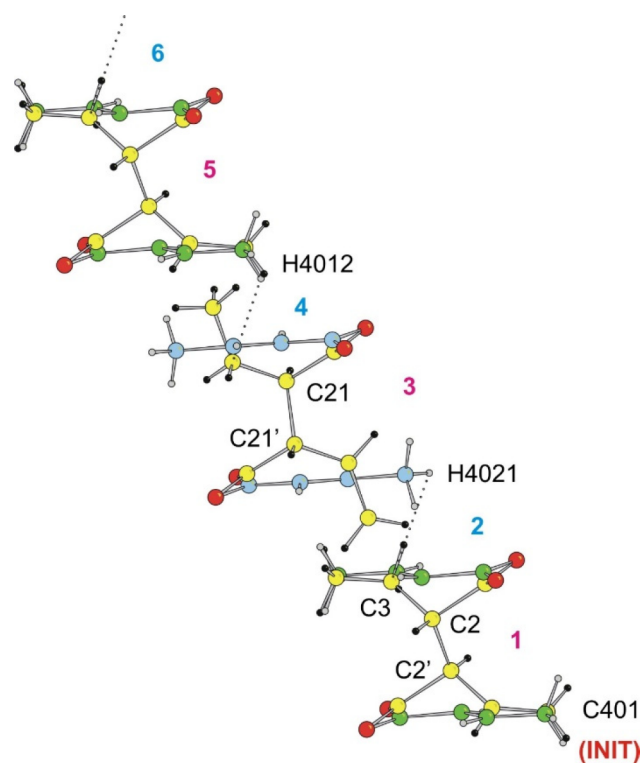


Figure 9. View of the set of superimposed major-component (top and bottom set) and minor-component (middle set, with blue C atoms for monomer) reactant/product molecules shown in Figure 6a, with each unit translated by one and two unit cells along the *a* direction, in order to show the likely geometrical mechanism of the radical chain reaction, as described in the text.

observed minor component reactivity. The analogous γ -carbon to γ -carbon atom C4...C41' ($1-x, -1-y, -1-z$) product "cross-contact", is quite normal at 3.759 Å. The diagram construction is somewhat more complicated, as this time we again search for the shortest β -carbon to methyl H distance in propagation step 2, but for both (i) the major product abstraction from the minor reactant, and (ii) the minor product abstraction from the major reactant. We find these distances to be (i) C3...H4021' ($1-x, -1-y, -1-z$) at a distance of 4.090 Å and (ii) C31 to H4012' ($1-x, -1-y, -1-z$) at a distance of 4.034 Å. These use a dimer molecule for C3 and C31, respectively, and monomer molecules for the hydrogen atom transfer. The analogous monomer–monomer and dimer–dimer distances for (i) are 4.045 and 4.043 Å, and for (ii) are 3.646 and 3.689 Å; we note that none of the contacts are unusually short.

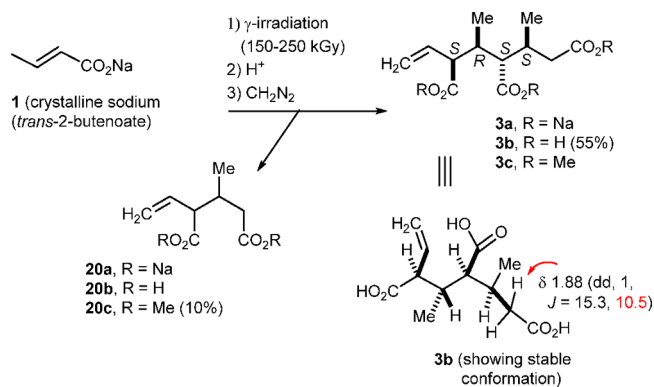
The complete relationship for the geometrical course of the mixed major–minor component "stack" is shown in Figure 9, and we may describe the process in a manner analogous to that for the major component. Note that the monomer molecules in the middle of the stack are the minor component, with C atoms colored blue; this pair will produce a minor component product, as shown. Initiation (INIT) occurs with breaking of a C401–H bond and formation of radical 18 (see Scheme 7) at atom C401. Propagation step 1 (label 1) involves bond formation between the α -carbon atoms (green color, just above and below the new bond) of the monomer to form the C2–C2' bond, along with the formation of radical 19 at atom C3. Propagation step 2 (label 2) involves the abstraction of hydrogen atom H4021 from a symmetry-related C402 atom (see above). Another radical 18 is created in step 2, and a second round of propagation begins with

the first step (label 3) forming a C21–C21' bond (the two blue monomer α -carbon atoms above and below C21 and C21' are the reacting atoms) and radical 19 at C31, followed by the second step 2 with abstraction of a H4012 atom from methyl carbon atom C401 (label 4). The third round of propagation begins in a like manner with bond formation and radical 19 generation (step 1, label 5) and the partially shown step 2 (label 6). The torsion angle of approach C2'–C2–C3...H4021 is 166.6°, and the torsion angle C21'–C21–C31...H4012 is 111.2°, both consistent with *anti*-addition.

The 4.521 Å distance between the carbon radical and the methyl hydrogen atom in propagation step 2 of the major–major reaction (and the analogous distances of 4.090 and 4.034 Å for the major–minor reaction) are much longer than those that we and others have observed in γ -ray initiated radical chain reactions as taken from monomer–monomer distances which are 3.13 Å for 4,³ 3.32 Å for 6,³ 3.31 or 3.55 Å for 8,⁴ 3.10 or 3.30 Å for 10,⁴ 3.09–3.30 Å for 2-deoxy- β -D-erythro-pentopyranose,⁴¹ 3.4 Å for D-fructose,³⁹ and 3.05–3.47 Å for a bis alkyne dimerization.^{42,63} The only other hydrogen atoms that can be abstracted by the alkyl radical of dimer 19 are either sp^2 hydrogen atoms (bond strength 111 kcal/mol) or water hydrogen atoms (bond strength 117 kcal/mol)⁶⁴ that are too strongly bound to be abstracted by an alkyl radical. It is likely that the radical has a long lifetime in the crystal. The monomer and dimer radical are not directly bound to magnesium but held more loosely in a cavity so greater molecular motion may be possible than is typical in solid-state reactions. Thus, in this case a shorter abstraction distance than that calculated from the crystal structure may be achieved.

⁶⁰Co γ -irradiation of Sodium *trans*-2-Butenoate (1). As we have previously communicated,¹ γ -irradiation of crystalline 1 followed by acidification with aqueous hydrochloric acid and filtration of the precipitate gave crude tricarboxylic acid 3b in 55% yield (see Scheme 8); the structure of 3b was determined

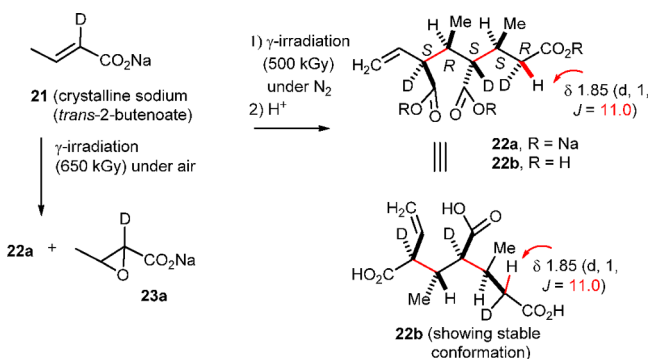
Scheme 8. γ -Ray-Induced Trimerization of 1



by X-ray crystallographic analysis. Crude acid 3b was treated with diazomethane⁶⁵ to form trimethyl ester 3c that was estimated to be 94% pure by GC analysis. The filtrate was concentrated after the removal of precipitated 3b, taken up in ether and treated with diazomethane to give a complex mixture consisting of additional 3c (57%), dimer 20c⁶⁶ (22%) with unknown stereochemistry, and numerous minor products. The total yield was determined to be 68% of 3c and 12% of 20c by GC analysis of the ester mixture obtained by concentration of the acidified mixture prior to filtration, dissolution in ether, and treatment with diazomethane.

The stereochemistry of the hydrogen atom transfer can be easily determined using deuterium-labeled *trans*-2-butenic acid as described above and in earlier papers in this series.^{3,4} We need to use *trans*-2-butenic-2-*d* acid[†] because the hydrogen atom is transferred to the 2-position rather than the 3-position as in the thermal dimerization of **1**. Crystalline sodium *trans*-2-butenate-2-*d* (**21**) was prepared and γ -irradiated in a partially filled vial under air to give a mixture containing approximately 60% of starting material, only 20% of **22a**, and 16% of sodium *trans*-2,3-epoxybutanoate-2-*d* (**23a**) (see Scheme 9).⁶⁷ The

Scheme 9. γ -Ray-Induced Trimerization of **21**

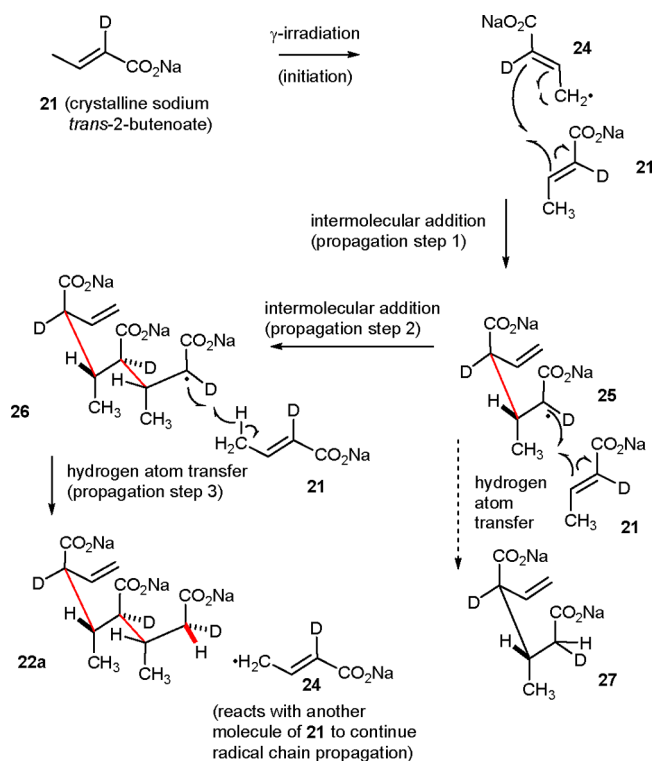


decreased yield and formation of the epoxide byproduct from reaction of oxygen with radical intermediates is expected for radical chain reactions. Epoxide formation is not observed in earlier studies because we used less-precious unlabeled *trans*-2-butenate compounds, and reactions were carried out in full, tightly packed, capped vials with little air space. Fortunately, γ -irradiation of a sample of **21** sealed under vacuum followed by acidification afforded a precipitate consisting of a 9:1 mixture of **22b** and unreacted *trans*-2-butenic-2-*d* acid. In the NMR spectrum of **22b** the vicinal coupling constant for the CHD proton to the adjacent methine hydrogen is 11 Hz, consistent with preferential conformations with the CO₂H group *anti* to the large R(CO₂H)CD substituent as shown.⁶⁸ This indicates that the hydrogen atom is transferred *anti* to the previously formed C–C bond.

The overall mechanism is shown in Scheme 10. γ -Irradiation of **21** leads to loss of a hydrogen atom to give allylic radical **24**, which adds to a second molecule of **21** to give dimeric radical **25** in the first propagation step. Addition of dimeric radical **25** to a third molecule of **21** *anti* to the previously formed C–C bond will give trimeric radical **26** in the second propagation step. In the third propagation step, trimeric radical **26** abstracts a hydrogen atom from a fourth molecule of **21** *anti* to the previously formed C–C bond to give product **22a** and another molecule of allylic radical **24**. This complex sequence of stereo- and regiospecific reactions likely occurs under topochemical control. The minor product dimer **27**, the deuterium-labeled analogue of **20a**, can be formed from dimeric radical **25** by hydrogen abstraction from **21**.

γ -Irradiation of compounds prepared from *trans*-2-butenic-4,4,4-*d*₃ acid should give analogous products in which a deuterium atom from the methyl group is transferred in the final propagation step. The spectra of these compounds should be informative because coupling to the methyl groups will be removed but all backbone hydrogen atoms will be present except for the one replaced by a deuterium atom. We prepared *trans*-2-butenic-4,4,4-*d*₃ acid in seven steps from Meldrum's acid and

Scheme 10. Radical Chain Mechanism for the Conversion of **21** to **22a**



trideuteroacetyl chloride.⁶⁹ Great care was needed throughout this process to prevent deuterium from washing out. Unfortunately, the γ -irradiation of the 4,4,4-trideuterated analogues of **1** and **12** proceeded in much lower yield than that of the unlabeled compounds and gave product mixtures that could not be analyzed completely.⁶⁹ γ -Irradiation with a deuterium atom at C₂ or C₃ should exhibit only small secondary isotope effects. Primary kinetic isotope effects as large as 15.9 have been reported for hydrogen atom transfer in radical chain reactions.⁷⁰ Presumably, because a deuterium atom must be transferred from the CD₃ group, the radical chain reaction no longer proceeds efficiently.

Structural Chemistry of Sodium *trans*-2-Butenoate (**1**)

While compound **1** may be prepared easily, the growth of single crystals remains a challenging project to this day. Over a period of three decades, many graduate and undergraduate research personnel were asked to participate in our quest to grow high-quality crystals. We had only three partially successful experiments, which, in part, helped us to understand the solid-state behavior of this remarkable material. We found two different structures, which, for the sake of simplicity, we will designate as polymorph **1**_I, and polymorph **1**_{II}; the latter polymorph was measured at 294 and 120 K, designated as RT and LT in Table 2. Compound **1** invariably crystallizes as a very thin, platelike material, a likely mixture of polytypes, resembling mica in appearance: layers of the material easily split off from the mass. Thus, one must be very careful in handling **1** in order to preserve any single-crystal character. The rare crystals of **1** are highly mosaic, with omega (Weissenberg or serial diffractometer) widths of up to 2°. Summary crystal data appear in Table 2; a full report appears in Table S3. The first-discovered phase, **1**_I, has a short *c*-axis of 3.465 Å. The second-discovered phase, **1**_{II}, has cell constants equal to those of polymorph **1** at 294 K, except that the *c*-axis is doubled and the space group has changed from

Table 2. Summary of Crystallographic Data for Crystal 1

compound_form	1_I	1_II(RT)	1_II(LT)
<i>a</i> (Å)	28.354(8)	28.334(3)	27.803 (7)
<i>b</i> (Å)	5.283(2)	5.2869(12)	5.2864(10)
<i>c</i> (Å)	3.465(1)	6.9224(17)	6.8607(15)
β (deg)	92.95(3)	93.007(13)	90.732(17)
<i>V</i> (Å ³)	518.3(3)	1035.6(4)	1008.3(4)
<i>Z</i> , <i>Z'</i>	4, 0.5	8, 1	8, 1
F.W. (g mol ⁻¹)	108.07	108.07	108.07
space group	<i>C2/m</i>	<i>C2/c</i>	<i>C2/c</i>
<i>T</i> (K)	294	294	120

C2/m to *C2/c*. Another crystal of **1_II** was found later and measured at 120 K. All three materials were far from ideal: **1_I** was triply twinned, with only partial resolution of the twinning, and had a high *R* value of 0.137; **1_II(RT)** had a high *R* value of 0.107 and reacted/decomposed (85.6%, decomposition correction applied) under Cu *K* α irradiation before a complete data set could be obtained. The best sample was twinned **1_II(LT)**, with *R* = 0.0692 and 100% completeness. Our experience over the long period of study indicates that **1** is a mixture of these two phases, and likely other polytypes. We therefore choose to base our discussion of the structural chemistry of the most well-defined material, polymorph **1_II**, with a limited, brief comparison to the structure of **1_I**.

The coordination environment of the sodium ion in polymorph **1_II** is shown in Figure 10. The Na ion is five-coordinate, with Na–O distances ranging from 2.337 to 2.424(3) Å, along with a longer contact of 2.638(3) Å to the apical O2 atom. Similar coordination for Na is also present in the closely related structures of sodium propynoate²³ (Na–O 2.368–2.494 Å; 3.120 Å to apical O2) and the β -polymorph of sodium acetate (Na–O 2.309–2.477 Å; 2.802 Å to apical O2).⁷¹ Coordination in the apical position is more symmetrical in **1_II** (2.424, 2.638 Å) than in the propynoate and acetate salts.

We note that the distance guidelines of the topochemical postulate for the onset and control of reactivity do not generally apply to thermal reactions,^{72–74} where reactive materials may have initial distances of ~ 5 Å.⁷² However, in cases such as the thermal dimerization of **1**, where the partner molecules are *already* within distances only slightly longer than a van der Waals contact, we can expect that topochemical control and least-motion considerations will prevail, and the product(s) will likely reflect the observed intermolecular relationships. In the case of **1**, however, the crystal structure of polymorph **1_I** suggests that **1** is disordered by 180° rotation about the C1–C2 bond (see Figure S2) so that dimer pairs with both eclipsed and alternating *trans*-2-butenates need to be considered.

As described earlier, heating solid **1** to 300 °C gives dimer **2a**, disodium *rel*-(3*S*,4*R*)-1-hexene-3,4-dicarboxylate, in 84% yield, by a thermal ene reaction (see Schemes 5 and 6).^{25,26} Compound **1** has short α -carbon atom C2...C2' (*x*, 2–*y*, *z*–1/2) contacts of 3.438(1) Å along the *c*-axis. Two such contacts (dotted lines) are shown in Figure 10. In order to obtain product **2a**, a rotation of 180° around the carboxylate carbon atom to α -carbon atom bond (C1–C2) must first occur. The reaction takes place at 300 °C, and a rotation, possibly accompanied by a phase transition, is thus plausible. Figure 11 shows a perspective view of the two *trans*-2-butenate anions at the bottom right of Figure 10 and shows why a rotation of 180° must first occur before a concerted ene reaction can occur. We can examine the likely transition states for the formation of either **2a** or the *rel*-

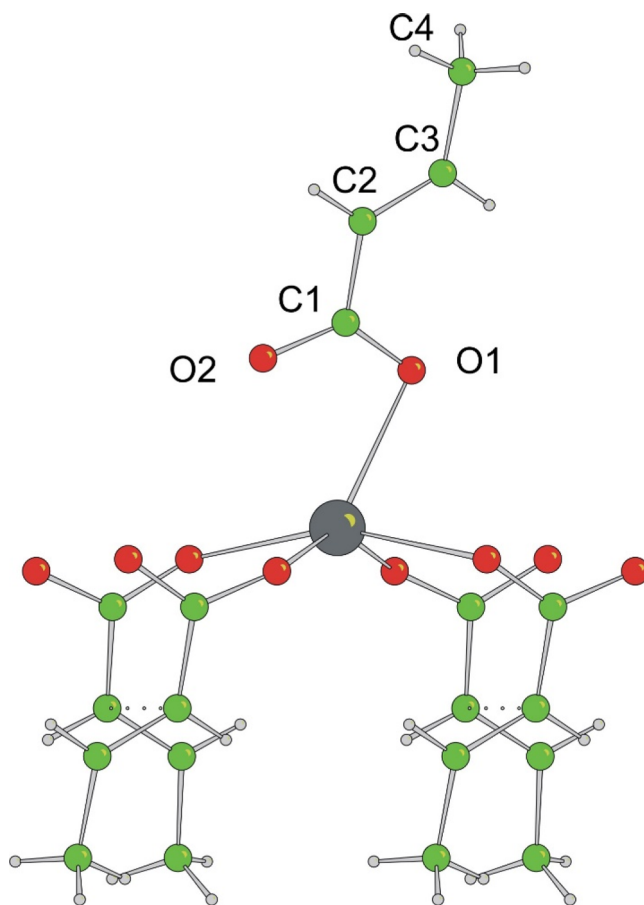


Figure 10. Coordination environment of the Na ion in polymorph **1_II**. Contacts of 3.438 Å between α -carbon atoms along the crystallographic *c*-axis are indicated by dotted lines. Note that the alkene bonds are alternating rather than eclipsed.

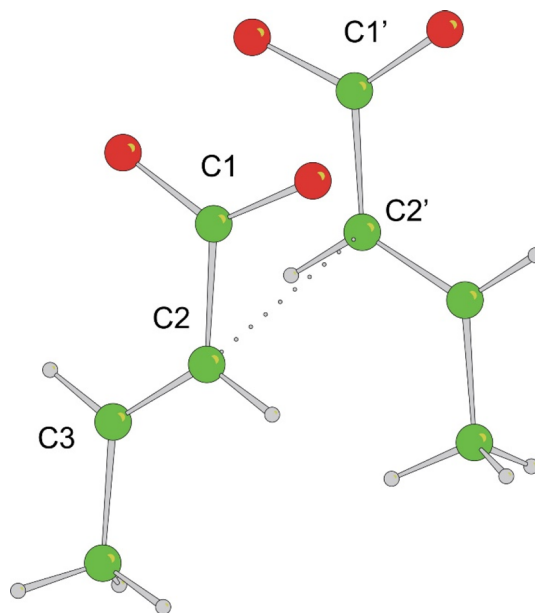


Figure 11. View of two nearest neighbors (cf. Figure 10) showing (dotted line) short C2–C2' contact of 3.438 Å. A rotation of 180° must occur around the C1'–C2' bond before a concerted ene reaction can occur. The C1–C2...C2'–C1' torsion angle is -8° . An analogous view of polymorph **1_I** may be viewed in Figure S3.

(3*R*,4*R*) diastereomer. In Figure 12, the left reaction shows the thermal ene dimerization of crystalline **1** with eclipsed *trans*-2-

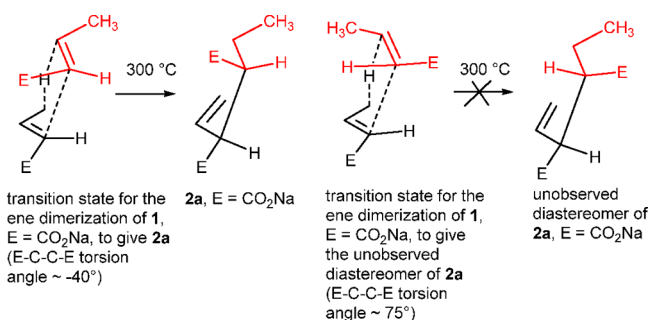


Figure 12. Left reaction shows the thermal ene dimerization of crystalline **1** with eclipsed *trans*-2-butenates after 180° rotation about the C1–C2 bond to give **2a**. The right reaction shows why the thermal ene dimerization of the conformer of **1** with alternating *trans*-2-butenates observed in the crystal structure does not give the diastereomer of **2a**.

butenates after 180° rotation about the C1–C2 bond to give **2a**. The C1–C2...C2'–C1' torsion angle in the transition state (i.e., the E–C...C–E torsion angle at left in Figure 12) is about -40°, a modest twist from the torsion angle of -8(3)° in the crystal structure of **1_II** (see Figure 11). The right reaction shows why the thermal ene dimerization of the conformer of **1** with alternating *trans*-2-butenates that is observed in the crystal structure does not give the diastereomer of **2a**. A C1–C2...C2'–C1' torsion angle of about 75° is required (cf. the E–C...C–E torsion angle at the right in Figure 12), and that is unlikely to be achieved in the crystal because it would require moving the carboxylate ions away from the sodium atoms.

A final note in this case concerns the crystal structure of triply twinned polymorph **1_I**. With a *c*-axis length of 3.465 Å, all molecules are expected to be eclipsed. As detailed in the Experimental Section, however, a further complication is that the molecule has crystallographic *m* symmetry, with the mirror plane containing the Na1, C1, and C2 atoms. With a 1:1 disorder, we do not know the disposition of a pair of adjacent reactant molecules with certainty (see Figures S2 and S3 for illustrations). With (a) the disorder, (b) the possibility of a high-temperature molecular reorientation, and (c) the complications arising from only partially corrected twinning, we will not consider polymorph **1_I** in the following discussion of the trimerization of **1**.

Finally, there remains the question of how the crystal structure of **1** helps us understand the γ -ray-induced trimerization reaction. The reaction occurs at ambient temperature, so that any molecular reorientation or phase transition is unlikely. For polymorph **1_II**, Figure 13 shows the bilayer packing and short intermolecular α -carbon to symmetry-related β' -carbon, C2...C3' ($x, 2-y, z-1/2$), contacts of 3.651(6) Å, all within one section of the bilayer. The *trans*-2-butenate moiety packs in a head-to-head arrangement, with C1 and C2 directly above and below the analogous carbon atoms along the *c*-axis; the alkene carbon bonds have an alternating orientation in a single section of the bilayer.

We can now consider the orientation of *trans*-2-butenates that leads to the observed product **3a** in the trimerization of **1**, which is clearly shown in Scheme 10. The first C–C bond in the trimer **3a** is formed from alternating *trans*-2-butenates as expected from the structure of polymorph **1_II**, but the second C–C bond is formed from eclipsed *trans*-2-butenate species. Unfortunately, the absence of a single-crystal-to-single-crystal reaction for **1** leaves us without enough information to explain the stereochemistry of the trimerization. One possibility is that 180° rotation about the C1–C2 bond to give the eclipsed species needed for the second addition occurs readily after the crystal structure is disrupted by the first addition, and the resultant molecular motion creates free space. We also cannot explain why the reaction is selective for trimer **3a** (68%) over dimer **20** (12%) and tetramers (5%).

CONCLUSION

Irradiation of metal *trans*-2-butenates with ⁶⁰Co γ -rays is a powerful synthetic tool for the chemo-, regio- and stereospecific preparation of dimers and trimers. In the present work, we have discovered a sixth product that can be formed selectively by a γ -ray-induced radical chain reaction of a crystalline alkali or alkaline earth *trans*-2-butenate.^{3,4} γ -Irradiation of crystalline hexaaquamagnesium *trans*-2-butenate dihydrate (**12**) affords *rel*-(3*S*,4*R*)-1-hexene-3,4-dicarboxylate (**2**) by a single-crystal-to-single-crystal reaction by *anti* addition to the butenolate double bond, as established by deuterium-labeling experiments. Naruchi reported that the same dicarboxylate **2** is formed by heating crystalline sodium *trans*-2-butenate (**1**) at 300 °C, but this thermal ene reaction has now been shown by deuterium labeling to proceed by *syn* addition to the butenolate double bond as expected. γ -Irradiation of sodium *trans*-2-butenate forms a single trimer chemo-, regio-, and stereospecifically, as demonstrated by using deuterium labeling to establish the

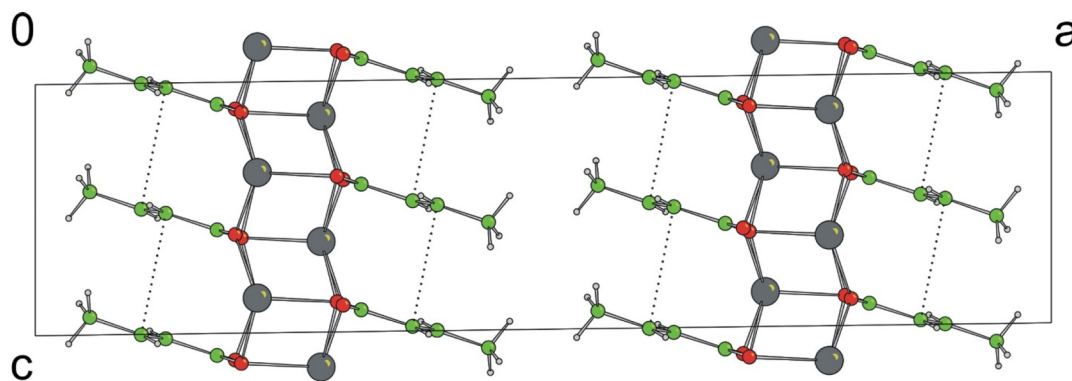


Figure 13. View of the packing of polymorph **1_II** viewed down the *b*-axis. The dotted lines show the favorable bilayer packing arrangement, and short C2...C3' ($x, 2-y, z-1/2$) contacts of 3.651 Å, each set within one section of the bilayer.

stereochemistry of hydrogen atom transfer. The crystal structure of sodium *trans*-2-butenolate has been determined, and the packing observed is consistent with the observed dimerization and γ -ray-induced trimerization. As we showed previously with the γ -irradiation of other *trans*-2-butenolates,^{3,4} the formation of the carbon–carbon bond and hydrogen atom transfer in the conversion of **12** to **2** is unequivocally topochemical, stereospecific, and not the result of a random process.

Apart from our work with *trans*-2-butenolates^{1–4} and early work with carbohydrates,^{36–41} there are no systematic studies of the chemo-, regio-, and stereospecific syntheses of small molecules using ionizing radiation. We hope that our studies will stimulate the search for new classes of these reactions.

EXPERIMENTAL SECTION

General Procedures. All commercially available reagents were used without further purification unless otherwise noted. NMR spectra were recorded in CDCl₃, D₂O (referenced to the peak of dioxane at δ 3.75, the peak of HDO at δ 4.79, or the peak of acetone at δ 2.08), or DMSO-*d*₆ (referenced to residual solvent at δ 2.50) on a 400 MHz spectrometer. The following abbreviations are used to indicate signal multiplicity: s, singlet; d, doublet; t, triplet; q, quartet; br, broad. Chemical shifts are reported in δ (ppm downfield from TMS) and coupling constants (*J* values) in Hz. A Gammacell 220 Irradiator (Atomic Energy of Canada, Ltd.), equipped with a ⁶⁰Co source, was used for γ -irradiation experiments. The nominal dose rate at the time of these experiments varied from 10 kGy as of January, 1991, to 2.5 kGy/day as of June, 2002 and 1.9 kGy/day as of April, 2004 because of the decay of ⁶⁰Co (half-life of 5.26 years). A ⁶⁰Co Gamma reactor at the University of Massachusetts, Lowell, nominal activity 18–20 kGy/h, was also used for γ -irradiation experiments.

Preparation of Hexaaquamagnesium *trans*-2-Butenoate Dihydrate (12**).** A stock solution of magnesium *trans*-2-butenolate was prepared using a 100 mL three-necked round-bottomed flask equipped with a thermometer, a condenser, and a stopper. The flask was charged with 30 mL of water and maintained at 75 °C using a heating mantle. *trans*-2-Butenoic acid (5.319 g, 61.8 mmol) was added slowly to the flask. (MgCO₃)₄Mg(OH)₂·5H₂O (3.000 g, 6.178 mmol) was added in several portions. Each time that the bubbling subsided, a new portion was added. After the addition was complete, the solution was stirred for 1 h at 75 °C. The solution was filtered through a preheated funnel (~75 °C) into a preheated flask to give an aqueous stock solution.

Upon slow evaporation at room temperature, two different types of crystals, prismatic **12** and plate-like **6**, grew within 1–2 weeks. Prismatic crystals of **12** were separated and used for the single-crystal-to-single-crystal dimerization studies.

Alternatively, the diffusion technique below was selective for the crystallization of **12** with several organic solvents and for the crystallization of **6** with DMF.³ The aqueous stock solution (1 mL) was placed in a Pyrex culture tube (18 × 150 mm). An organic solvent (5 or 10 mL of ethyl acetate, cyclohexane, hexanes, ethyl ether, or benzene) was layered carefully with a syringe on the top of the aqueous solution and the tube was capped tightly. After 1–2 d, prismatic crystals of **12** were formed. In optimal cases, 81 mg (23%) for ethyl acetate, 37 mg (11%) for ethyl ether, and 28 mg (8%) for hexanes were obtained from the 1:10 mixtures of aqueous stock solution and organic solvent. Addition of either 5 or 10 mL of acetone or acetonitrile to the 1 mL of aqueous stock solution resulted in the formation of **12**, **6**, or a mixture of both as could be determined by visual inspection of the crystals. Although the use of these solvents did not lead exclusively to **12**, the yields of crystalline material were much higher than with other organic solvents (276 mg with 5 mL of acetonitrile and 201 mg with 5 mL of acetone).

γ -Irradiation of **12. Magnesium *rel*-(3*S*,4*R*)-1-Hexene-3,4-dicarboxylate (**2b**).** Samples of **12** were irradiated in capped vials under air for 2–128 d at 5 kGy/day. The samples were dissolved in D₂O and analyzed by ¹H NMR. The spectra showed increased conversion of

12 to **2b** over time: 2 d (0%), 4 d (1.8%), 8 d (7.4%), 16 d (23.1%), 32 d (45.5%), 64 d (65.6%), and 128 d (80.3%). The spectrum of **2b** was determined from the 45.5:54.5 mixture of **2b** and **12** obtained after 32 d of γ -irradiation: ¹H NMR (D₂O) 5.82 (dd, 1, *J* = 17.2, 10.4, 10.1), 5.10 (br d, 1, *J* = 17.2), 5.02 (br d, 1, *J* = 10.1), 2.88 (dd, 1, *J* = 10.4, 10.4), 2.37 (ddd, 1, *J* = 10.4, 10.4, 4.6), 1.52–1.34 (m, 2), 0.86 (t, 3, *J* = 7.3); ¹³C NMR 184.0 (C), 182.8 (C), 137.8 (CH), 117.3 (CH₂), 59.4 (CH), 55.6 (CH), 25.3 (CH₂), 12.8 (CH₃).

After longer γ -irradiation times, trace impurities were seen in the spectra: (the percent is relative to **2b** as 100%) δ 2.88 (8%, dd, 1, *J* = 11.6, 9.2), 2.55 (<1%, dd, 1, *J* = 10, 10), 0.98 (2%, d, 3, *J* = 7.3), 0.90 (5%, d, 3, *J* = 6.1), 0.83 (4%, d, 3, *J* = 7.5).

An authentic sample of the sodium *rel*-(3*S*,4*R*)-1-hexene-3,4-dicarboxylate (**2a**) was prepared by heating sodium *trans*-2-butenolate (**1**) at 300 °C as described by Naruchi.^{25,26} The ¹H NMR spectrum of a mixture of **2a** and **2b** indicated the presence of a single dicarboxylate.

Preparation of Dimethyl *rel*-(3*S*,4*R*)-1-Hexene-3,4-dicarboxylate (2d**).** A sample of irradiated **12** (250 mg, 1.48 mmol) was dissolved in 10 mL of 1 M HCl. The solution was extracted with five 10 mL portions of CH₂Cl₂. The combined organic layers containing acid **2c** were dried (MgSO₄), filtered, and treated dropwise with diazomethane in ether.⁶⁵ When the yellow color of diazomethane persisted, dilute aqueous acetic acid was added and the solution was washed with water, dried (MgSO₄), and concentrated to give 69.4 (47%) of **2d** as an oil: ¹H NMR 5.78 (ddd, 1, *J* = 17.1, 9.6, 9.5) 5.16 (br d, 1, *J* = 17.1), 5.12 (br d, 1, *J* = 9.6), 3.67 (s, 3), 3.63 (s, 3), 3.22 (dd, 1, *J* = 9.5, 9.5), 2.76 (ddd, 1, *J* = 9.5, 9.5, 4.7), 1.65–1.58 (m, 1), 1.48–1.39 (m, 1), 0.87 (t, 3, *J* = 7.4); ¹³C NMR (CDCl₃) 173.8 (C), 172.6 (C), 133.3 (CH), 119.0 (CH₂), 52.6 (CH), 52.0 (CH₃), 51.4 (CH₃), 49.6 (CH), 23.7 (CH₂), 11.7 (CH₃). A sample of **2a** prepared by heating **1** was converted to dimethyl ester **2d** with identical ¹H and ¹³C NMR spectra.

Preparation of Sodium *trans*-2-Butenoate-3-*d* (14**).** A solution of *trans*-2-butenic-3-*d* acid³ (300 mg, 3.44 mmol) in 4 mL of H₂O was neutralized with 3 M NaOH to the phenolphthalein end-point. The solution was evaporated at 20 Torr until cloudy. Acetone (6 mL) was added to precipitate a transparent, cellophane-like polycrystalline material. The precipitate was isolated by vacuum filtration, washed with acetone, and dried in vacuum over P₂O₅ to give 240 mg (64%) of sodium *trans*-2-butenolate-3-*d* (**14**): ¹H NMR (D₂O, referenced to internal dioxane at δ 3.75) 5.81 (s, 1), 1.79 (s, 3).

Pyrolysis of **14. Preparation of Disodium *rel*-(3*S*,4*R*,5*S*)-1-Hexene-3,4-dicarboxylate-2,5-*d*₂ (**15**).** A sample of sodium *trans*-2-butenolate-3-*d* (75 mg, **14**) was placed in a 3 mm inside diameter glass tube and packed tightly using a glass rod. A septum was placed at the rim of the glass tube, and the sample was evacuated for 3 min. The sample was then placed under nitrogen for 3 min and sealed using an air/gas flame. The tube was heated at 300 °C for 4 h, taken out of the oven, and allowed to cool to room temperature to give 68 mg of white solid. NMR analysis of a small amount of product (10 mg) indicated that the solid consisted of 45% unreacted **14** and 55% of disodium *rel*-(3*S*,4*R*,5*S*)-1-hexene-3,4-dicarboxylate-2,5-*d*₂ (**15**): ¹H NMR (D₂O, referenced to internal dioxane at δ 3.75) 5.09 (s, 1), 5.01 (s, 1), 2.87 (d, 1, *J* = 11.6), 2.37 (dd, 1, *J* = 11.6, 3.6), 1.38 (qd, 1, *J* = 7.3, 3.6), 0.85 (d, 3, *J* = 7.3).

Preparation of Hexaaquamagnesium *trans*-2-Butenoate-3-*d* Dihydrate (16**).** A solution of *trans*-2-butenic-3-*d* acid³ (1.00 g, 11.5 mmol) in 6 mL of H₂O was warmed to 75 °C, and (MgCO₃)₄·Mg(OH)₂·5H₂O (557 mg, 1.15 mmol) was added in small portions. Once addition was complete, the reaction mixture was heated at 75 °C for 1 h and cooled to room temperature, and excess (MgCO₃)₄·Mg(OH)₂·5H₂O was removed by gravity filtration. A portion (1 mL) of the filtrate was placed in a test tube, and then a layer of less dense solvent was carefully added with a syringe on the top of the aqueous solution. The tube was capped tightly and kept at 0 °C for 2 d. The weight of crystalline **16** varied using different solvents: acetone, 250 mg; ethyl ether, 67 mg; hexanes, 40 mg; 85 mg of crystal can be obtained without adding a second solvent: ¹H NMR (D₂O, referenced to internal dioxane at δ 3.75) 5.70 (s, 3), 1.67 (s, 1).

γ -Irradiation of **16. Magnesium (3*S*,4*R*,5*R*)-1-Hexene-3,4-dicarboxylate-2,5-*d*₂ (**17**).** Crystalline magnesium *trans*-2-bute-

noate-3-*d* (40 mg, 16) was placed in a 3 mm inside diameter glass tube and packed tightly using a glass rod. A septum was placed at the rim of the glass tube, and the sample was evacuated for 3 min. The sample was then placed under nitrogen for 3 min and sealed using an air/gas flame. Several tubes prepared in this manner were subjected to γ -rays. The tubes were periodically removed from the γ -ray irradiator and NMR analysis of product indicated that the solid consisted of unreacted starting material and the magnesium *rel*-(3*S*,4*R*,5*R*)-1-hexene-3,4-dicarboxylate-2,5-*d*₂ (17). The conversion was about 3% after 12 d, 28% after 30 d, and 53% after 90 d (1.9 kGy/d). Data for salt 17 were determined from the mixture: ¹H NMR (D₂O, referenced to internal dioxane at δ 3.75) 5.09 (s, 1), 5.02 (s, 1), 2.88 (d, 1, *J* = 11.0), 2.37 (dd, 1, *J* = 11.0, 11.0), 1.41 (qd, 1, *J* = 7.3, 11.0), 0.85 (d, 3, *J* = 7.3).

X-ray Data Collections for Pristine and Irradiated Hexa-aquamagnesium *trans*-2-Butenoate Dihydrate (12). Initial experiments suggested that, unlike other metal *trans*-2-butenate materials we studied, 12 undergoes a crystal-to-crystal solid-state reaction.^{1–4} The experimental plan involved using six crystals, with the hope that three to four would survive the required months of γ -irradiation without degradation (dehydration-cum-loss of crystal quality had been previously observed). Six crystals were selected and coated with perfluoropolyether (Riedel-de Haën, RS 3000). The coated crystals were then placed into glass capillaries (Charles Supper Company), affixed to the capillary walls with epoxy and the capillaries sealed using a hot wire. The capillaries were then set into specially designed 1/8 in. brass pins, modeled after those used in the early Philips *PAILRED* diffractometer (Figure 14). The capillaries were epoxied to the pin at the

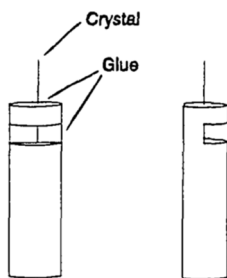


Figure 14. Glass capillary mounting pin used in this work.

drilled opening, and also at a milled-out opening halfway down the pin body. One side of the pin had previously been milled flat so that the crystal and its pin could be removed for placement in the irradiator, and later replaced in the goniometer with the setscrew against the flat surface, such that the original orientation matrix could be used to quickly align the crystal and begin a data collection. At the time of this experimental work, a CCD machine was not available in our laboratory, nor was a low-temperature device. Data were collected at RT on an Enraf-Nonius CAD-4 Turbo diffractometer equipped with Mo *K α* radiation. After data collection, crystals were irradiated for various times with ⁶⁰Co γ -rays at Brandeis University (Gammacell 220 Irradiator, as described in the main paper), and two crystals were given a further dose of 650 kGy at University of Massachusetts, Lowell. A summary of experimental details appears in Tables 1A and 1B, and full data for crystals 1–4 appear in Tables S2_0 through S2_110_65m.

A total of 26 structure determinations were carried out (4 crystals \times 6 irradiation periods + 2 crystals \times 1 irradiation at University of Massachusetts, Lowell). The careful reader will notice that around/after the 16-day irradiation point, the unit cell axes, which have been undergoing small changes, change from their original order of $a < b < c$ to $a < b > c$. CheckCIF assigns an Alert C error (“The unit cell is not reduced”) at this time, but of course we need to retain the original axis setting in order to provide a straightforward comparison of each stage of the reaction. All operations were performed on an Enraf-Nonius CAD-4 Turbo diffractometer, using a normal-focus sealed tube (graphite-monochromated Mo *K α* radiation). A 1.0 mm collimator was used for all experiments, as crystals were large (0.6–0.8 mm) and could not be cut without shattering. All diffractometer manipulations were carried

out using the Enraf-Nonius EXPRESS software,⁷⁵ while data reduction and absorption corrections were performed using the Enraf-Nonius MolEN package.⁷⁶ Cell constants were obtained using the SET4 procedure (25 reflections).⁷⁷ Data collection was carried out at 294 K. Completeness for all data collections was 100%. From the systematic absences, the observed metric constants, and intensity statistics, space group *P1* was considered initially; subsequent solution and refinement confirmed the correctness of this choice. The asymmetric unit of the pristine crystal contains one-half of a hexaaquamagnesium cation, one hydrate water molecule, and one disordered *trans*-butenoate anion (for the title complex, *Z'* = 0.5). The structure was solved using SIR-92⁷⁸ and refined (full-matrix-least-squares) using the Oxford University *Crystals for Windows* program.⁷⁹ All non-hydrogen atoms were refined using anisotropic displacement parameters. After location of H atoms on difference maps, H atoms attached to O were refined using isotropic displacement parameters, while H atoms attached to C were fixed at calculated positions and refined using riding constraints.⁸⁰ The solution and refinement process is of two types: (i) two-component disorder of reactant butenoates in the four pristine crystals and (ii) four-component disorder for all of the remaining 22 refinements; there are two disordered orientations of reactant butenoates as before, but now there are also two orientations of product hexenedicarboxylates (see Figures 5 and 6 in the main text). For the pristine crystals the only constraint needed was that the sum of the occupancies of the two disordered butenoates sum to 1.0. For the remaining 22 determinations, three general restraints, as described in Results and Discussion, ensured a stable and consistent refinement. The restraint that the ratio of major/minor product occupancies and the ratio of major/minor reactant occupancies are expected to be equal was tested by a free refinement of the two ratios; no significant difference was observed. Additionally, a small number (*ca.* 10–15) of distance and angle restraints (but no vibrational parameter restraints) were used in all of the four-component disorder refinements (*i.e.*, all of the crystals irradiated with γ -rays). Results of the refinements may be seen in the tables cited, and additional details of the standard geometric restraints applied appear in the individual CIF files.

Preparation of Sodium *trans*-2-Butenoate (1). A solution of *trans*-2-butenic acid (3.000 g, 34.8 mmol) in 20 mL of H₂O was neutralized with 3.0 M sodium hydroxide to the phenolphthalein endpoint. The solution was concentrated under reduced pressure (20 Torr) until a cloudy mixture formed. Acetone (25 mL) was added to precipitate a transparent, cellophane-like polycrystalline material. The precipitate was isolated by filtration, washed with acetone, and dried in vacuo (0.25 Torr) over CaSO₄ to afford 3.748 g (99.6%) of 1: ¹H NMR (D₂O) 6.65 (dq, 1, *J* = 15.5, 6.8), 5.83 (dq, 1, *J* = 15.5, 1.6), 1.79 (dd, 3, *J* = 6.8, 1.6); IR (KBr) 3040, 1660, 1560, 970 cm⁻¹.

γ -Irradiation of 1. Preparation of *rel*-(2*S*,3*S*,4*R*,5*S*)-2,4-Dimethyl-6-heptene-1,3,5-tricarboxylic Acid (3b). Salt 1 (3.24 g, 29.9 mmol) was γ -irradiated for 13 d (150–250 kGy). The resulting colorless powder was dissolved in water (20 mL) to give a homogeneous solution that was acidified with concentrated hydrochloric acid (3.5 mL) to give a colorless precipitate. The precipitate was isolated by filtration and dried in vacuo (0.25 Torr) over CaSO₄ to give 1.40 g (55%) of 3b as a colorless powder. mp 203–205 °C; ¹H NMR (DMSO-*d*₆) 12.2 (s, 3, OH), 5.85 (ddd, 1, *J* = 16.5, 10.9, 8.6), 5.11 (br d, 1, *J* = 10.9), 5.10 (dd, 1, *J* = 16.5, 2.9), 2.89 (dd, 1, *J* = 8.6, 6.4), 2.37–2.29 (m, 3), 2.10 (ddq, 1, *J* = 6.4, 7.1, 7.1), 1.88 (dd, 1, *J* = 15.3, 10.5), 0.95 (d, 3, *J* = 6.7), 0.93 (d, 3, *J* = 6.7); ¹³C NMR (DMSO-*d*₆) 174.8 (C), 173.8 (C), 173.4 (C), 136.0 (CH), 117.5 (CH₂), 53.9 (CH), 52.2 (CH), 36.6 (CH₂), 35.4 (CH), 28.3 (CH), 19.1 (CH₃), 13.3 (CH₃); IR (KBr) 1721, 1706, 990, 906 cm⁻¹. Anal. Calcd for C₁₂H₁₈O₆: C, 55.81; H, 7.02. Found: C, 56.08; H, 7.05. Irradiation of the peak at δ 2.89 changed the peaks at δ 5.85 (dd, 1, *J* = 16.5, 10.9) and 2.10 (dq, 1, *J* = 7.1, 7.1). Irradiation of the peak at δ 2.10 changed the peaks at 2.89 (d, 1, *J* = 8.6), 2.33 (sharper), and 0.93 (s, 3).

Trimethyl *rel*-(2*S*,3*S*,4*R*,5*S*)-2,4-Dimethyl-6-heptene-1,3,5-tricarboxylate (3c). A solution of triacid 3b (0.180 g, 0.698 mmol) in 5 mL of isopropanol was treated with diazomethane in ether⁶⁵ until the light-yellow color of diazomethane persisted. The solution was dried (MgSO₄) and concentrated in vacuo to afford 205 mg (98%) of

3c as a colorless oil: mp 27–30 °C; $^1\text{H NMR}$ (CDCl_3) 5.89 (ddd, 1, $J = 17.0, 10.3, 9.0$), 5.16 (br d, 1, $J = 10.3$), 5.13 (br d, 1, $J = 17.0$), 3.68 (s, 3), 3.67 (s, 3), 3.65 (s, 3), 2.99 (dd, 1, $J = 9.0, 5.9$), 2.56–2.34 (m, 3), 2.29 (ddq, 1, $J = 5.9, 6.7, 6.7$), 2.09 (dd, 1, $J = 15.3, 10.6$), 1.02 (d, 3, $J = 6.8$), 0.98 (d, 3, $J = 6.4$); $^{13}\text{C NMR}$ 174.2 (C), 173.5 (C), 173.0 (C), 134.6 (CH), 118.6 (CH_2), 54.6 (CH), 53.1 (CH), 51.7 (CH_3), 51.6 (CH_3), 51.1 (CH_3), 36.2 (CH_2), 21.8 (CH), 19.2 (CH_3), 14.2 (CH_3); IR (neat) 3080, 1745, 1740, 1640, 995, 915 cm^{-1} .

Analysis of **3c** by capillary GC (Heliflex, 30 m \times 0.25 mm; 60–150 °C at 10 degrees/min, 5 min isothermal, 150–190 °C at 20 degrees/min, 8 min isothermal; detector temperature 280 °C, injector temperature 240 °C) gave 6 peaks (% of total integration): 11.8 min (1%), 12.4 min (94%, **3c**), 12.8 min (2%), 14.0 min (1%), 15.0 min (1%), and 15.8 min (2%). This indicates that crude **3c** is 94% pure and that triacid **3b** precipitates in similar purity.

Gas Chromatographic Analysis of γ -Irradiated 1. Another irradiated sample of **1** was acidified, concentrated without removal of the precipitated **3b**, taken up in ether, and treated with diazomethane to give a mixture of methyl esters. GC analysis as above gave 8 peaks (% of total integration): 4.6 min (0.4%), 5.2 min (12%, **20c**), 5.7 min (1.2%), 11.8 min (6%), 12.4 min (68%, **3c**), 12.8 min (7%), 15.0 min (2%), and 15.8 min (3%). Samples eluting at 4.6–5.8 min (100–120 °C) are dimers; samples eluting at 11.8–12.8 min (150 °C) are trimers, and samples eluting at 15.0–15.8 min (150–170 °C) are tetramers. Capillary GC analysis of methyl 3-hydroxybutanoate (4.8 min), diester **2d** (4.9 min), dimethyl (*E*)-2-ethylidene-3-methylpentandioate (5.3 min),⁶⁶ and dimethyl (*Z*)-2-ethylidene-3-methylpentandioate (7.2 min)⁶⁶ gave peaks distinct from those observed in the chromatograms obtained from samples of irradiated **1**. A sample of both diastereomers of dimethyl 2-ethenyl-3-methylpentandioate (**20c**)⁶⁶ eluted with the major byproduct at 5.2 min in the samples of irradiated **1**. Therefore, acid **3b** is the major product (68%) and precipitates selectively upon acidification.

The mother liquor resulting from acidification of irradiated **1** and removal of the precipitated **3b** by filtration was concentrated, taken up in ether, and treated with diazomethane to give a mixture of methyl esters. GC analysis as above gave 8 peaks (% of total integration): 4.6 min (1%), 5.2 min (22%, **20c**), 5.7 min (1%), 11.8 min (5%), 12.4 min (57%, **3c**), 12.8 min (11%), 15.0 min (1%), and 15.8 min (2%). Not all of the triacid **3b** precipitates upon acidification because it is still the major product in solution after removal of all the precipitated **3b**.

Preparation of Sodium *trans*-2-Butenoate-2-*d* (21**).** *trans*-2-Butenoic-2-*d* acid[†] (1.00 g, 12 mmol) was dissolved in 20 mL of water and sodium hydroxide (0.47 g, 12 mmol) was added. The reaction mixture was stirred at room temperature for 1 h and concentrated under reduced pressure to give a colorless solid that was washed with acetone to remove any excess acid and dried to give 1.2 g (96%) of **21** as a colorless solid, mp >220 °C.

γ -Irradiation of **21 Under Nitrogen. Preparation of *rel*-(**1R,2S,3S,4R,5S**)-2,4-Dimethyl-6-heptene-1,3,5-tricarboxylic-1,3,5-*d*₃ Acid (**22b**).** Crystalline **21** (100 mg, 0.90 mmol) was placed in a 3 mm inside diameter glass tube and packed tightly using a glass rod. A septum was placed at the rim of the glass tube, and the sample was evacuated for 3 min. The sample was then placed under nitrogen for 3 min and sealed using an air/gas flame. The sample was subjected to 500 kGy (25 h, University of Massachusetts, Lowell) γ -rays. The product was isolated by dissolving the sample in 2 mL of water and adding a few drops of concentrated hydrochloric acid to form a colorless precipitate that was collected and dried to give 11 mg of a 9:1 mixture of triacid **22b** and unreacted acid *trans*-2-butenoic-2-*d* acid as a colorless solid: $^1\text{H NMR}$ ($\text{DMSO-}d_6$) 5.83 (dd, 1, $J = 10.4, 17.0$), 5.10 (br d, 1, $J = 10.4, 1.8$), 5.09 (dd, 1, $J = 17.0, 1.8$), 2.22 (dq, 1, $J = 11, 6.7$), 2.07 (q, 1, $J = 6.9$), 1.85 (d, 1, $J = 11.0$), 0.933 (d, 3, $J = 6.9$), 0.918 (d, 3, $J = 6.7$). Residual peaks for *trans*-2-butenoic-2-*d* acid were observed at δ 6.81–6.86 (m, 1) and 1.83 (d, 3, $J = 6.7$). Irradiation of the peak at δ 0.91 showed NOEs to the peaks at δ 1.85, 2.07, 2.22. Irradiation of the peak at δ 2.07 showed an NOE to the peak at δ 0.918. Irradiation of peak at δ 2.22 showed NOEs to the peaks at δ 1.85 (small), 0.918, and 0.933. Irradiation of the peak at δ 5.83 showed NOEs to the peaks at δ 5.09 and 5.10.

γ -Irradiation of **21 Under Air.** Crystalline **21** (100 mg, 0.90 mmol) was placed in a glass vial, capped, and subjected to 650 kGy (32.5 h, University of Massachusetts, Lowell) γ -rays. A 10 mg portion of the sample was dissolved in water and acidified with concentrated HCl (2 drops). No precipitate was observed. Another 10 mg of sample was dissolved in D_2O for NMR analysis. Integration of the spectrum indicated that the major component (60%) was starting material **21**. Approximately 21% of trimer **22a** was also observed. Another product (16%) was sodium *trans*-2,3-epoxybutanoate-2-*d* (**23a**): $^1\text{H NMR}$ (D_2O) 3.10 (q, 1, $J = 4.9$), 1.33 (d, 3, $J = 4.9$). This data matches the published data for the potassium salt of *trans*-2,3-epoxybutanoate:⁶⁷ $^1\text{H NMR}$ (D_2O) 3.17 (d, 1, $J = 2.4$), 3.11 (dq, 1, $J = 2.4, 5.1$), 1.35 (d, 3, $J = 5.1$). Finally, other peaks (4–5%) were observed from uncharacterized products: $^1\text{H NMR}$ (D_2O) 4.59 (d, $J = 6.1$), 4.21 (d, $J = 4.2$), 1.17 (d, 3, $J = 6.7$).

Preparation and Crystal Growth for Polymorphs of Sodium *trans*-2-Butenoate (1**).** **Form 1_I.** Sodium *trans*-2-butenoate was readily prepared by neutralizing a solution of *trans*-2-butenoic acid with NaOH (1 M) to the phenolphthalein end-point. The solubility was assessed, and numerous methods for crystal growth were attempted, including crystallization from water and methanol as well as mixtures of those solvents with EtOH, DMSO, DMF, triethylene glycol, acetone, CHCl_3 , and Et_2O . Methods included slow evaporation between –10 and 50 °C, doping (dyestuffs) of aqueous solutions,⁸¹ evaporation at reduced pressure, and crystal growth in gels/Sephadex G-25. The highest-quality crystals were obtained by slow evaporation of a 1:1 H_2O :DMSO solution at room temperature. Salt **1** is highly soluble in H_2O (solubility = 720 g L^{-1}), and nucleation almost invariably occurs at the solution surface. The result is very thin “cellophane-like” crystals with a high degree of mosaicity ($\omega \approx 2^\circ$ from Weissenberg photography). The chosen mixed solvent system appears to decrease the rate of crystallization, and thus, higher-quality crystals form.

Form 1_II (for Room-Temperature Structure Determination). Sodium hydroxide (0.80 g, 20 mmol) was added to a stirred solution of *trans*-2-butenoic acid (1.96 g, 20 mmol) in 40 mL of 1:1 EtOH: H_2O . The mixture was stirred at 25 °C for 4 h and filtered. The filtrate was placed in a 100 mL glass crystallizing dish and allowed to evaporate at RT. The dish was covered with a Kimwipe held in place with a rubber band. Several holes were punctured in the Kimwipe with a needle. Crystals of **1_II** are very thin and fragile, so extra care was needed to avoid deformation. Colorless thin plate-like crystals were observed on the surface of the solution after 2 weeks. The crystals were carefully removed from the glass dish using a spatula and dried on filter paper.

Form 1_II (for Low-Temperature Structure Determination). Sodium hydroxide (0.811 g, 0.0203 mol) was dissolved in 40 mL of a 1:1 mixture of ethanol and H_2O . To the solution, 1.958 g (0.0227 mol) of *trans*-2-butenoic acid and 3 mL of dimethyl sulfoxide were added; the reaction mixture was stirred for 4 h, filtered, and allowed to evaporate slowly. Colorless, very thin film-like crystals of Form **1_II** were obtained from the top of the solution after 3 weeks of slow-evaporation. The crystals were carefully transferred to a glass slide and immediately covered with Paratone oil prior to the X-ray analysis.

X-ray Data Collection, Solution, and Refinement for 1_I. All operations were performed on a Syntex P2₁ serial diffractometer, a graphite-monochromator, and normal-focus, sealed tube Mo $K\alpha$ radiation. A 1.5 mm collimator was used for all experiments, as the crystals were large (max. dimension *ca.* 1.2 mm), mica-like in appearance and physical nature, and could not be cut without deformation. Data collection was carried out at 294 K. All diffractometer manipulations, including data collection, integration, scaling, and absorption corrections, were carried out using the Syntex data collection software.⁸² Initial data reduction, absorption corrections, solution, and refinement were performed using the Syntex XTL package on a Nova 1200 32k computer.⁸³ Completeness was 100%. From the systematic absences, the observed metric constants and intensity statistics, space groups $P2_1$ or $P2_1/m$ (both with $Z' = 2$) were considered initially. However, while a plausible structure was obtained, refinements would not yield *R* factors below *ca.* 22%. Further work on the problem was abandoned at that time. We decided to re-examine the data and solution at the time that this paper was in preparation. We

observed the tell-tale signature of twinning in a plot of F_o versus F_c and noted both (a) that many of the $h + k$ odd reflections were weak and (b) that the two “independent” molecules in the asymmetric unit were almost perfectly C -centered. A reasonable hypothesis appeared to be that the crystals were twinned and that the lattice was NOT primitive, rather C -centered, with $h + k$ odd reflections nonzero owing to twinning and/or stacking faults. Accordingly, the space group was changed to $C2/m$, which has one-half molecule in the asymmetric unit ($Z = 4$; $Z' = 0.5$), with the Na atom and the C1–C2 bond residing on the crystallographic mirror plane, and the β - and γ -carbon (C3 and C4) atoms disordered. The data were then analyzed using ROTAX;⁸⁴ a TLQS twin⁸⁵ with three twin laws was found: in addition to the parent crystal, a 180° rotation about (100) or [502]⁸⁶ and an obliquity^{85,86} of 0.15° and a rotation about [413] or (100) with an obliquity of 3.52° were chosen and refined with the constraint that the scale factors for the three twin laws sum to 1.0. At the conclusion of the refinement, the twin laws and their occupancies were ([100/010/001], 0.703(2); [0.980 0.497 1.491/0.017 -0.996 0.013/0.010 0.002 -0.993] 0.089(2); [1 0 0.843/0 -1 0/0 0 -1], 0.208(2)). The structure was solved using SIR-92⁷⁸ and refined on F (full-matrix least-squares) using the Oxford University CRYSTALS for Windows package.⁷⁹ All non-hydrogen atoms were refined using anisotropic displacement parameters. After location of H atoms on difference maps, H atoms were initially refined with soft restraints on the bond lengths and angles to regularize their geometry (C–H in the range 0.93–0.98 Å) and $U_{\text{iso}}(\text{H})$ (in the range of 1.2–1.5 times U_{eq} of the parent atom); then H atom positions were refined by using riding constraints.⁸⁰ The final R value including the $h + k$ odd data is 0.1376, a decrease of ca. 9% from the previous solution. R for the $C2/m$ model without the $h + k$ odd reflections is 0.0672, suggesting that the twin model is incomplete, but likely represents the major chemical features of the structure. R for the model refined with I_{obs} filtering is 0.0870,⁸⁷ which, once again, suggests an incomplete model. The final file is available in the deposited CIF files.

X-ray Data Collection, Solution, and Refinement for 1_II at Room Temperature. All diffractometer manipulations were carried out at 294 K on a CAD-4U diffractometer, equipped with graphite-monochromator and a normal-focus Cu $K\alpha$ sealed tube. Data collection was managed with the Enraf-Nonius EXPRESS software,⁷⁵ while data reduction and absorption corrections were performed using the Enraf-Nonius MolEN package.⁷⁶ Cell constants were obtained using the SET4 procedure (25 reflections).⁷⁷ From the systematic absences, the observed metric constants, and intensity statistics, space group $C2/c$ was chosen initially; subsequent solution and refinement confirmed the correctness of this choice. Inspection of the three standard reflections indicated that the crystal had decayed dramatically (intensity decreased by 85.6%) during the data collection; a decay correction was applied during data reduction, but the data collection had to be abandoned at ca. 75% completeness; additional suitable crystals were not available. The structure was solved using SIR-92⁷⁸ and refined (F , full-matrix-least-squares) using the Oxford University Crystals for Windows program.⁷⁹ The asymmetric unit contains one molecule of the title complex ($Z = 8$; $Z' = 1$). Although a plot of F_o versus F_c suggested twinning was present, either trying a few low-obliquity laws observed in other crystals or using ROTAX⁸⁴ failed to find any applicable twin laws. No twinning was observed. After location of H atoms on electron-density difference maps, the H atoms were initially refined with soft restraints on the bond lengths and angles to regularize their geometry (C–H in the range 0.93–0.98 Å and $U_{\text{iso}}(\text{H})$ in the range 1.2–1.5 times U_{eq} of the parent atom), after which the positions were refined with riding constraints.⁸⁰ The final least-squares refinement converged to $R = 0.1073$ ($I > 1.96\sigma(I)$, 373 data) and $R_w = 0.2638$ (F , 841 data, 65 parameters). The final CIF is available in the deposited CIF files. This determination, with its faults, is included to provide evidence of the similarity in cell constants of Polymorphs 1_I and 1_II. No significant differences were observed between the distances and angles observed for 1_II at 294 and 120 K.

X-ray Data Collection, Solution, and Refinement for 1_II at Low Temperature. All operations were performed on a Bruker-Nonius Kappa Apex2 diffractometer, using graphite-monochromated Mo $K\alpha$ radiation. All diffractometer manipulations, including data

collection, integration, scaling, and absorption corrections, were carried out using the Bruker Apex2 software.⁸⁸ Preliminary cell constants were obtained from three sets of 12 frames. Data collection was carried out at 120 K, using a frame time of 40 s and a detector distance of 60 mm. The optimized strategy used for data collection consisted of two phi and two omega scan sets, with 0.5° steps in phi or omega; completeness was 100.0%. A total of 1730 frames were collected. Final cell constants were obtained from the xyz centroids of 402 reflections after integration. From the systematic absences, the observed metric constants and intensity statistics, space group $C2/c$ was chosen initially; subsequent solution and refinement confirmed the correctness of this choice. The structure was solved using SIR-92,⁷⁸ and refined (F^2 , full-matrix-least-squares) using the Oxford University Crystals for Windows program.⁷⁹ The asymmetric unit contains one molecule of the title complex ($Z = 8$; $Z' = 1$). Refinement led quickly to a final R value of 0.0857; however, a plot of F_o versus F_c suggested that the crystal was a twin. The structure was then analyzed using ROTAX;⁸⁴ a TLQS twin⁸⁵ with a 180° rotation about [100]⁸⁶ and an obliquity^{85,86} of 0.732° was chosen and refined with the constraint that the scale factors for the two twin laws sum to 1.0. At the conclusion of the refinement, the twin laws and their occupancies were ([1 0 0/0 1 0/0 0 1], 0.939(6); [1 0 0/0 -1 0/-0.006 0 -1], 0.061(6)). After location of H atoms on electron-density difference maps, the H atoms were initially refined with soft restraints on the bond lengths and angles to regularize their geometry (C–H in the range of 0.93–0.98 Å and $U_{\text{iso}}(\text{H})$ in the range 1.2–1.5 times U_{eq} of the parent atom), after which the positions were refined with riding constraints.⁸⁰ The atom C1 was refined by using a thermal similarity restraint to atom C2. The final least-squares refinement converged to $R = 0.0692$ ($I > 2\sigma(I)$, 416 data) and $R_w = 0.1172$ (F^2 , 794 data, 65 parameters). The final CIF is available in the deposited CIF files.

■ ASSOCIATED CONTENT

Supporting Information

The Supporting Information is available free of charge at <https://pubs.acs.org/doi/10.1021/acs.cgd.0c01466>.

Figures S1 through S3; Tables S1, S2_0 through S2_110_65m, S3; correspondence between structure ID and CCDC number (Table S4); ^1H NMR spectra of 2a, 3b, 15, 17, and 22b (PDF).

Figures 5 and 6.pptx: animations of the “before and after” positions for the major and minor organic reactants and products from γ -irradiation of crystalline hexaaquamagnesium *trans*-2-butenate dihydrate (ZIP)

Mechanism.pptx: animations of the radical chain mechanism for the major and minor organic reactants and products from γ -irradiation of crystalline hexaaquamagnesium *trans*-2-butenate dihydrate (ZIP)

Accession Codes

CCDC 2039295–2039323 contain the supplementary crystallographic data for this paper. These data can be obtained free of charge via www.ccdc.cam.ac.uk/data_request/cif, or by emailing data_request@ccdc.cam.ac.uk, or by contacting The Cambridge Crystallographic Data Centre, 12 Union Road, Cambridge CB2 1EZ, UK; fax: +44 1223 336033.

■ AUTHOR INFORMATION

Corresponding Authors

Barry B. Snider – Department of Chemistry, Brandeis University, Waltham, Massachusetts 02453-2728, United States; orcid.org/0000-0002-2680-6104; Email: snider@brandeis.edu

Bruce M. Foxman – Department of Chemistry, Brandeis University, Waltham, Massachusetts 02453-2728, United States; orcid.org/0000-0001-5707-8341; Email: foxman1@brandeis.edu

Authors

Wen Shang – Department of Chemistry, Brandeis University, Waltham, Massachusetts 02453-2728, United States;

orcid.org/0000-0002-6984-3060

Roxana F. Schlam – Department of Chemistry, Brandeis University, Waltham, Massachusetts 02453-2728, United States; orcid.org/0000-0003-3322-1750

Magali B. Hickey – Department of Chemistry, Brandeis University, Waltham, Massachusetts 02453-2728, United States

Jingye Zhou – Department of Chemistry, Brandeis University, Waltham, Massachusetts 02453-2728, United States

Kraig A. Wheeler – Department of Chemistry, Brandeis University, Waltham, Massachusetts 02453-2728, United States; orcid.org/0000-0001-6752-7542

Graciela C. Diaz de Delgado – Department of Chemistry, Brandeis University, Waltham, Massachusetts 02453-2728, United States; orcid.org/0000-0001-5511-4230

Chun-Hsing Chen – Department of Chemistry, Brandeis University, Waltham, Massachusetts 02453-2728, United States; orcid.org/0000-0003-0150-9557

Complete contact information is available at:
<https://pubs.acs.org/10.1021/acs.cgd.0c01466>

Notes

The authors declare no competing financial interest.

ACKNOWLEDGMENTS

We thank Dr. David Watkin and Professor Richard Cooper of Oxford University for helpful discussions and guidance on complex refinement issues involving disorder and twinning, Professor Gerhard Wegner of the Max Planck Institut für Polymerforschung for stimulating discussions and suggestions which led to the deuterium-labeling experiments, the late Professor Howard Flack of the University of Geneva for helpful discussions on twinning, and the late Professor Dan Sandman for facilitating the use of the ^{60}Co γ -irradiator at the University of Massachusetts, Lowell. The work described here spanned three decades and was supported in part by the National Science Foundation, Grants DMR 8812417, 9221487, 9629994, 0089257, and 0504000; we are most grateful for that support.

REFERENCES

- (1) Diaz de Delgado, G. C.; Wheeler, K. A.; Snider, B. B.; Foxman, B. M. Stereospecific, γ -Ray-Induced Trimerization of Crystalline Sodium *trans*-2-Butenoate. *Angew. Chem., Int. Ed. Engl.* **1991**, *30*, 420–422.
- (2) Cho, T. H.; Chaudhuri, B.; Snider, B. B.; Foxman, B. M. Stereospecific γ -ray-induced dimerization of crystalline bis(*trans*-but-2-enoato)calcium. *Chem. Commun.* **1996**, 1337–1338.
- (3) Hickey, M. B.; Schlam, R. F.; Guo, C.; Cho, T. H.; Snider, B. B.; Foxman, B. M. Stereospecific solid-state cyclodimerization of bis(*trans*-2-butenoato)calcium and triaquabis(*trans*-2-butenoato)magnesium. *CrystEngComm* **2011**, *13*, 3146–3155.
- (4) Shang, W.; Hickey, M. B.; Enkelmann, V.; Snider, B. B.; Foxman, B. M. Chemo- and stereospecific solid-state dimerization of lithium *trans*-2-butenoate and lithium *trans*-2-butenoate formamide solvate. *CrystEngComm* **2011**, *13*, 4339–4350.
- (5) Cohen, M. D.; Schmidt, G. M. J.; Sonntag, F. I. Topochemistry. Part II. The photochemistry of *trans*-cinnamic Acids. *J. Chem. Soc.* **1964**, 2000–2013.
- (6) Schmidt, G. M. J. Topochemistry. Part III. The crystal chemistry of some *trans*-cinnamic acids. *J. Chem. Soc.* **1964**, 2014–2021.

(7) Enkelmann, V.; Wegner, G.; Novak, K.; Wagener, K. B. Single-Crystal-to-Single-Crystal Photodimerization of Cinnamic Acid. *J. Am. Chem. Soc.* **1993**, *115*, 10390–10391.

(8) Abdelmoty, I.; Buchholz, V.; Di, L.; Guo, C.; Kowitz, K.; Enkelmann, V.; Wegner, G.; Foxman, B. M. Polymorphism of Cinnamic and α -Truxillic Acids: New Additions to an Old Story. *Cryst. Growth Des.* **2005**, *5*, 2210–2217.

(9) Amjaour, H.; Wang, Z.; Mabin, M.; Puttkammer, J.; Busch, S.; Chu, Q. R. Scalable preparation and property investigation of a *cis*-cyclobutane-1,2-dicarboxylic acid from β -*trans*-cinnamic acid. *Chem. Commun.* **2019**, *55*, 214–217.

(10) MacGillivray, L. R.; Papaefstathiou, G. S.; Frišić, T.; Hamilton, T. D.; Bučar, D.-K.; Chu, Q.; Varshney, D. B.; Georgiev, I. G. Supramolecular Control of Reactivity in the Solid State: From Templates to Ladderanes to Metal-Organic Frameworks. *Acc. Chem. Res.* **2008**, *41*, 280–291.

(11) Lu, Y.; Bolokowicz, A. J.; Reeb, S. A.; Wiseman, J. D.; Wheeler, K. A. Chiral transmission to crystal photodimerizations of leucine-methionine quasaracemic assemblies. *RSC Adv.* **2014**, *4*, 8125–8131.

(12) Sherman, D. A.; Murase, R.; Duyker, S. G.; Gu, Q.; Lewis, W.; Lu, T.; Liu, Y.; D'Alessandro, D. M. Reversible single crystal-to-single crystal double [2 + 2] cycloaddition induces multifunctional photo-mechano-electrochemical properties in framework materials. *Nat. Commun.* **2020**, *11*, 2808.

(13) Rath, B. B.; Vittal, J. J. Single-Crystal-to-Single-Crystal [2 + 2] Photocycloaddition Reaction in a Photosensitive One-Dimensional Coordination Polymer of Pb(II). *J. Am. Chem. Soc.* **2020**, *142*, 20117–20123.

(14) Khan, S.; Dutta, B.; Mir, M. H. Impact of solid-state photochemical [2 + 2] cycloaddition on coordination polymers for diverse applications. *Dalton Trans.* **2020**, *49*, 9556–9563.

(15) Morawetz, H.; Rubin, I. D. Polymerization in the crystalline state. II. Alkali acrylates and methacrylates. *J. Polym. Sci.* **1962**, *57*, 669–686.

(16) Heyman, J. B.; Chen, C.-H.; Foxman, B. M. Crystal Structures of Missing Links in the Early History of Solid-State Reactions: The Group IA Acrylates and Methacrylates. *Cryst. Growth Des.* **2020**, *20*, 330–336.

(17) Enkelmann, V. Structural aspects of the topochemical polymerization of diacetylenes. *Adv. Polym. Sci.* **1984**, *63*, 91–136.

(18) Ogawa, T. Diacetylenes in polymeric systems. *Prog. Polym. Sci.* **1995**, *20*, 943–985.

(19) Lauher, J. W.; Fowler, F. W.; Goroff, N. S. Single-Crystal-to-Single-Crystal Topochemical Polymerizations by Design. *Acc. Chem. Res.* **2008**, *41*, 1215–1229.

(20) Hall, A. V.; Yufit, D. S.; Apperley, D. C.; Senak, L.; Musa, O. M.; Hood, D. K.; Steed, J. W. The crystal engineering of radiation-sensitive diacetylene cocrystals and salts. *Chem. Sci.* **2020**, *11*, 8025–8035.

(21) Matsumoto, A.; Furukawa, D.; Mori, Y.; Tanaka, T.; Oka, K. Change in Crystal Structure and Polymerization Reactivity for the Solid-State Polymerization of Muconic Esters. *Cryst. Growth Des.* **2007**, *7*, 1078–1085.

(22) Furukawa, D.; Matsumoto, A. Reaction Mechanism Based on X-ray Crystal Structure Analysis during the Solid-State Polymerization of Muconic Esters. *Macromolecules* **2007**, *40*, 6048–6056.

(23) Jaufmann, J. D.; Case, C. B.; Sandor, R. B.; Foxman, B. M. Structure and γ -Ray Induced Solid-State Polymerization of Sodium Propynoate: Influence of Bilayer Formation on Solid-State Reactivity. *J. Solid State Chem.* **2000**, *152*, 99–104 and references therein.

(24) Vela, M. J.; Buchholz, V.; Enkelmann, V.; Snider, B. B.; Foxman, B. M. Solid-state polymerization of bis(3-butenoato)zinc: synthesis of a stereoregular oligomer. *Chem. Commun.* **2000**, 2225–2226.

(25) Naruchi, K.; Tanaka, S.; Yamamoto, M.; Yamada, K. Thermal Dimerization of Sodium Crotonate in a Solid State. *Nippon Kagaku Kaishi* **1983**, 1291–1293.

(26) Naruchi, K.; Miura, M. Thermal dimerization of alkali-metal salts of crotonic acid in the solid state. *J. Chem. Soc., Perkin Trans. 2* **1987**, *2*, 113–116.

(27) Foxman, B. M.; Vela, M. J. Reactive Crystals: Design and Discovery. *Trans. Am. Cryst. Assn.* **1998**, *33*, 75–84.

- (28) Vela, M. J.; Foxman, B. M. Bilayer formation in metal carboxylate structures: results from the Cambridge Structural Database. *Cryst. Eng.* **2000**, *3*, 11–31.
- (29) Groom, C. R.; Bruno, I. J.; Lightfoot, M. P.; Ward, S. C. The Cambridge Structural Database. *Acta Crystallogr., Sect. B: Struct. Sci., Cryst. Eng. Mater.* **2016**, *B72*, 171–179 ConQuest Version 2020.2.0.
- (30) Barja, B.; Aramendia, P.; Baggio, R.; Garland, M. T.; Peña, O.; Perec, M. Europium(III) and terbium(III) *trans*-2-butenates: syntheses, crystal structures, and properties. *Inorg. Chim. Acta* **2003**, *355*, 183–190.
- (31) Brodtkin, J. S.; Foxman, B. M.; Clegg, W.; Cressey, J. T.; Harbron, D. R.; Hunt, P. A.; Straughan, B. P. Preparation, Structure and Solid State Reactivity of Lanthanum Propynoates. *Chem. Mater.* **1996**, *8*, 242–247.
- (32) Clegg, W.; Little, I. R.; Straughan, B. P. Zinc Carboxylate Complexes: Structural Characterization of the Mixed-Metal Linear Trinuclear Complexes $MZn_2(\text{crot})_6(\text{base})_2$ ($M = \text{Mn, Co, Ni, Zn, Cd, Mg, Ca, Sr}$; $\text{crot}^- = \text{crotonate}(1^-)$; $\text{base} = \text{quinoline, 6-methylquinoline}$). *Inorg. Chem.* **1988**, *27*, 1916–1923.
- (33) Yang, L.; Foxman, B. M. Crystal and Molecular Structure of Ammonium *trans*-2-Butenoate, and a Preliminary Investigation of its Solid-State Reactivity. *Mol. Cryst. Liq. Cryst.* **2006**, *456*, 25–33.
- (34) Harada, J.; Ogawa, K.; Tomoda, S. Molecular Motion and Conformational Interconversion of Azobenzenes in Crystals as Studied by X-ray Diffraction. *Acta Crystallogr., Sect. B: Struct. Sci.* **1997**, *53*, 662–672.
- (35) Harada, J.; Ogawa, K. Pedal motion in crystals. *Chem. Soc. Rev.* **2009**, *38*, 2244–2252.
- (36) von Sonntag, C. Free-Radical Reactions of Carbohydrates as Studied by Radiation Techniques. In *Adv. Carbohydr. Chem. Biochem.*; Tipson, R. S., Horton, D., Eds.; Academic: New York, 1980; Vol. 37, pp 7–77.
- (37) von Sonntag, C.; Dizdaroglu, M. Radiation Chemistry of Carbohydrates. Part I. Radical Chain Reactions in Crystalline α -Lactose Monohydrate. *Z. Naturforsch., B: J. Chem. Sci.* **1973**, *28*, 367–368.
- (38) Kawakishi, S.; Kito, Y.; Namiki, M. Formation of 1-Deoxy-D-threo-2,5-Hexodiulose by Radiation Induced Chain Reaction in Crystalline D-Fructose. *Agric. Biol. Chem.* **1975**, *39*, 1897–1898.
- (39) Dizdaroglu, M.; Leitich, J.; von Sonntag, C. Conversion of D-Fructose into 6-Deoxy-D-threo-2,5-hexodiulose by γ -Irradiation: A Chain Reaction in the Crystalline State. *Carbohydr. Res.* **1976**, *47*, 15–23.
- (40) Dizdaroglu, M.; Henneberg, D.; Neuwald, K.; Schomburg, G.; von Sonntag, C. Radiation Chemistry of Carbohydrates, X. γ -Radiolysis of Crystalline D-Glucose and D-Fructose. *Z. Naturforsch., B: J. Chem. Sci.* **1977**, *32*, 213–224.
- (41) Schuchmann, M. N.; von Sonntag, C.; Tsay, Y.-H.; Krüger, C. Crystal Structure and the Radiation-Induced Free-Radical Chain Reaction of 2-Deoxy- β -D-erythro-pentopyranose in the Solid State. *Z. Naturforsch., B: J. Chem. Sci.* **1981**, *36*, 726–731.
- (42) Yamamoto, Y.; Ueda, T.; Kanehisa, N.; Miyawaki, K.; Takai, Y.; Tagawa, S.; Sawada, M.; Kai, Y. Selective Dimerization by a Radical Chain Reaction in γ -Irradiated Crystals of 1,3-Bis(3-acetoxyprop-1-ynyl)-4-methoxy-6-methylbenzene. *J. Chem. Soc., Perkin Trans. 2* **1997**, *2*, 743–747.
- (43) Chaudhary, A.; Mohammad, A.; Mobin, S. M. Recent Advances in Single-Crystal-to-Single-Crystal Transformation at the Discrete Molecular Level. *Cryst. Growth Des.* **2017**, *17*, 2893–2910.
- (44) Naumov, P.; Karothu, D. P.; Ahmed, E.; Catalano, L.; Commins, P.; Mahmoud Halabi, J.; Al-Handawi, M. B.; Li, L. The Rise of the Dynamic Crystals. *J. Am. Chem. Soc.* **2020**, *142*, 13256–13272.
- (45) Njus, J. M.; Sae-Lim, C.; Sandman, D. J. The interaction of cinnamic acids with ^{60}Co gamma radiation. *Mol. Cryst. Liq. Cryst.* **2006**, *456*, 55–61.
- (46) Chapiro, A.; Lahav, M.; Schmidt, G. M. J. Dimerization and polymerization of some disubstituted dienes in the crystalline state by the action of γ and ultraviolet rays. *C. R. Seances Acad. Sci., Ser. C* **1966**, *262*, 872–874. *Chem. Abstr.* **1966**, *65*, 12665.
- (47) Lahav, M.; Schmidt, G. M. J. Topochemistry. Part XXIII. The Solid-state Photochemistry at 25° of Some Muconic Acid Derivatives. *J. Chem. Soc. B* **1967**, 312–317.
- (48) Kropp, P. J.; Krauss, H. J. Photochemistry of Cycloalkenes. IV. Comparison with Crotonic Acid. *J. Org. Chem.* **1967**, *32*, 3222–3223.
- (49) Fausto, R.; Kulbida, A.; Schrems, O. UV-induced Isomerization of (*E*)-Crotonic Acid. Combined Matrix-isolated IR and *ab initio* MO Study. *J. Chem. Soc., Faraday Trans.* **1995**, *91*, 3755–3770.
- (50) MMX calculations were carried out with conformational searching using PCmodel version 8.0 from Serena Software. For **15**, the calculated coupling constants for $\text{H}_3\text{--H}_4$ and $\text{H}_4\text{--H}_5$ are 10.5 and 4.0 Hz, respectively, and the observed coupling constants are 11.6 and 3.6 Hz. For **17**, the calculated coupling constants for $\text{H}_3\text{--H}_4$ and $\text{H}_4\text{--H}_5$ are 10.5 and 10.3 Hz, respectively, and the observed coupling constants are 11.0 and 11.0 Hz.
- (51) Kraszni, M.; Szakács, Z.; Noszál, B. Determination of rotamer populations and related parameters from NMR coupling constants: a critical review. *Anal. Bioanal. Chem.* **2004**, *378*, 1449–1463.
- (52) Oba, M.; Miyakawa, A.; Shionoya, M.; Nishiyama, K. Synthesis of L-[4,5,5,5-D₄]Issoleucine: Determination of Approximate Rotamer Population about the $\text{C}_\beta\text{--C}_\gamma$ Bond. *J. Labelled Compd. Radiopharm.* **2001**, *44*, 141–147 The coupling constant for $\text{CD}_3\text{CHDC}(\text{H})\text{MeCHNH}_2\text{CO}_2\text{H}$ in the two diastereomers is 4.0 and 9.2 Hz, which corresponds well to the observed values of 3.6 and 11.0 Hz in **15** and **17**, respectively.
- (53) Hart, D. J.; Krishnamurthy, R. Investigation of a Model for 1,2-Asymmetric Induction in Reactions of α -Carbalkoxy Radicals: A Stereochemical Comparison of Reactions of α -Carbalkoxy Radicals and Ester Enolates. *J. Org. Chem.* **1992**, *57*, 4457–4470.
- (54) The methine proton adjacent to the carboxylic acid of 2-ethyl-3-methyl-3-phenylbutanoic acid absorbs at δ 2.59 (dd, 1, $J = 11.9$ and 2.8 Hz) with very different coupling constants to the methylene protons of the ethyl group at δ 1.17–1.25 and 1.57–1.65.⁵⁵ However, the methine proton adjacent to the ester of *t*-butyl 2-ethyl-3-methylbutanoate absorbs at δ 1.88 (ddd, 1, $J = 7.8, 7.8, 6.5$ Hz) with very similar coupling constants to the methylene protons of the ethyl group which both absorb at δ 1.53.⁵⁶ Observing very dissimilar coupling constants to the methylene protons of an ethyl group requires both (a) a strong conformational preference for one of the three staggered conformations and (b) significantly different chemical shifts for the methylene protons as in **2** (**15**, **17**) and the phenylbutanoic acid (11.9, 2.8 Hz) above. If the methylene protons have almost identical chemical shifts, non-first-order effects perturb the observed coupling constants, even if there is a conformational preference as in the *t*-butyl ester above (7.8 and 6.8 or 7.5 Hz). For real coupling constants of 10.0 and 4.0 Hz to the methylene protons of an ethyl group, the observed coupling constants will be 9.5 and 4.5 Hz if the methylene protons of the ethyl group are separated by 0.05 ppm at 400 MHz, but 7.9 and 6.1 Hz if the methylene protons of the ethyl group are separated by only 0.01 ppm at 400 MHz.
- (55) Zask, A.; Birnberg, G.; Cheung, K.; Kaplan, J.; Niu, C.; Norton, E.; Suayan, R.; Yamashita, A.; Cole, D.; Tang, Z.; Krishnamurthy, G.; Williamson, R.; Khafizova, G.; Musto, S.; Hernandez, R.; Annable, T.; Yang, X.; Discifani, C.; Beyer, C.; Greenberger, L. M.; Loganzo, F.; Ayral-Kaloustian, S. Synthesis and Biological Activity of Analogues of the Antimicrotubule Agent *N*, β , β -Trimethyl-L-phenylalanyl-N-[(1*S*,2*E*)-3-carboxy-1-isopropylbut-2-enyl]-N¹,3-dimethyl-L-valinamide (HTI-286). *J. Med. Chem.* **2004**, *47*, 4774–4786.
- (56) Studte, C.; Breit, B. Zinc-Catalyzed Enantiospecific $\text{sp}^3\text{--sp}^3$ Cross-Coupling of α -Hydroxy Ester Triflates with Grignard Reagents. *Angew. Chem., Int. Ed.* **2008**, *47*, 5451–5455.
- (57) Chan, E.; Foxman, B. M. Unpublished observations.
- (58) Ebersson, L. Studies on Succinic Acids. I. Preparation of α,α' -Dialkyl- and Tetraalkyl-Substituted Succinic Acids by Kolbe Electrolysis. *Acta Chem. Scand.* **1959**, *13*, 40–49.
- (59) Aslam, N. A.; Babu, S. A.; Sudha, A. J.; Yasuda, M.; Baba, A. Chelation-controlled diastereoselective construction of *N*-aryl-, *N*-acyl/tosylhydrazono β -substituted aspartate derivatives via Barbier-type reaction. *Tetrahedron* **2013**, *69*, 6598–6611.

- (60) Shimada, S.; Saigo, K.; Hashimoto, Y.; Maekawa, Y.; Yamashita, T.; Yamamoto, T.; Hasegawa, M. Diastereoselective Claisen Condensation-Type Reactions of Alkyl 2,2-Dialkoxycyclopropanecarboxylates with Esters and Acid Chlorides Promoted by Titanium(IV) Chloride. *Chem. Lett.* **1991**, *20*, 1475–1478.
- (61) Burtin, G.; Corringer, P.-J.; Hitchcock, P. B.; Young, D. W. Stereoselective Synthesis of β -Substituted Aspartic Acids via Tetrahydro-1,3-oxazin-6-ones. *Tetrahedron Lett.* **1999**, *40*, 4275–4278.
- (62) Lindsay Smith, J. R.; Nagatomi, E.; Stead, A.; Waddington, D. J. The autoxidation of aliphatic esters. Part 3. The reactions of alkoxy and methyl radicals, from the thermolysis and photolysis of peroxides, with neopentyl esters. *J. Chem. Soc., Perkin Trans.* **2001**, *2*, 1527–1533.
- (63) Reference 42 reports much longer distances, but the authors have reported distances from the radical center to the carbon of the CH, not from the hydrogen atom that is transferred. We recalculated those distances using their deposited CIF file.
- (64) Ruscic, B.; Wagner, A. F.; Harding, L. B.; Asher, R. L.; Feller, D.; Dixon, D. A.; Peterson, K. A.; Song, Y.; Qian, X.; Ng, C.-Y.; Liu, J.; Chen, W.; Schwenke, D. W. On the Enthalpy of Formation of Hydroxyl Radical and Gas-Phase Bond Dissociation Energies of Water and Hydroxyl. *J. Phys. Chem. A* **2002**, *106*, 2727–2747.
- (65) Arndt, F. Diazomethane. *Org. Synth.* **1935**, *15*, 3–5. (see note 3).
- (66) Alcock, S. G.; Baldwin, J. E.; Bohlmann, R.; Harwood, L. M.; Seeman, J. I. On the Conjugative Isomerizations of β,γ -Unsaturated Esters. Stereochemical Generalizations and Predictions for 1,3-Prototropic Shifts under Basic Conditions. *J. Org. Chem.* **1985**, *50*, 3526–3535.
- (67) Glabe, A. R.; Sturgeon, K. L.; Ghizzoni, S. B.; Musker, W. K.; Takahashi, J. N. Novel Functionalized Acylphosphonates as Phosphonofosphate Analogs. *J. Org. Chem.* **1996**, *61*, 7212–7216.
- (68) MMX calculations were carried out with conformational searching using PCmodel version 8.0 from Serena Software. For **22b**, the calculated vicinal coupling constant CHD-CH of 9.9 Hz is close to the observed coupling constant of 11.0 Hz. The calculated vicinal CHD-CH coupling constant for the diastereomer is 3.1 Hz.
- (69) Zhou, J. Studies of Solid-State Reactivity of α,β -Unsaturated Carbonyl Compounds. Total Syntheses of Lanopylin B1 and Sch 642305. Synthesis of the Alkenyl Substituted Tetracyclic Core of the Bisabosquols. Approaches to the Synthesis of Berkelic Acid. Ph.D. Thesis, Brandeis University, 2007.
- (70) Muchalski, H.; Levonyak, A. J.; Xu, L.; Ingold, K. U.; Porter, N. A. Competition H(D) Kinetic Isotope Effects in the Autoxidation of Hydrocarbons. *J. Am. Chem. Soc.* **2015**, *137*, 94–97.
- (71) Helmholdt, R. B.; Sonneveld, E. J.; Schenk, H. *Ab initio* crystal structure determination of β -sodium acetate from powder data. *Z. Kristallogr. - Cryst. Mater.* **1998**, *213*, 596–598.
- (72) Cheng, K.; Foxman, B. M. Polymerization of $\text{NiBr}_2[\text{P}(\text{CH}_2\text{CH}_2\text{CN})_3]_2$: A “Triply-Specific” Solid-State Reaction. *J. Am. Chem. Soc.* **1977**, *99*, 8102–8103.
- (73) Wheeler, K. A.; Foxman, B. M. Structure and Solid-State Reactivity of 2-Aminopyridinium Propynoate. *Chem. Mater.* **1994**, *6*, 1330–1336.
- (74) Di, L.; Foxman, B. M. The Solid-State Polymerization of Styryl Monomers: A Structural Perspective. *Supramol. Chem.* **2001**, *13*, 163–174.
- (75) Straver, L. H. *CAD4-EXPRESS*; Enraf-Nonius: Delft, The Netherlands, 1992.
- (76) Fair, C. K. *MolEN, An Interactive Structure Solution Procedure*; Enraf-Nonius: Delft, The Netherlands, 1990.
- (77) Schagen, J. D.; Straver, L.; van Meurs, F.; Williams, G. *CAD4 Version 5.0*; Enraf-Nonius, Delft, The Netherlands, 1989; Chapter X, p 10.
- (78) Altomare, A.; Cascarano, G.; Giacovazzo, G.; Guagliardi, A.; Burla, M. C.; Polidori, G.; Camalli, M. SIR92 - A Program for Automatic Solution of Crystal Structures by Direct Methods. *J. Appl. Crystallogr.* **1994**, *27*, 435.
- (79) Betteridge, P. W.; Carruthers, J. R.; Cooper, R. I.; Prout, K.; Watkin, D. J. *Crystals* Version 12: Software for Guided Crystal Structure Analysis. *J. Appl. Crystallogr.* **2003**, *36*, 1487.
- (80) Cooper, R. I.; Thompson, A. L.; Watkin, D. J. *CRYSTALS Enhancements: Dealing with Hydrogen Atoms in Refinement*. *J. Appl. Crystallogr.* **2010**, *43*, 1100–1107.
- (81) Buckley, H. E. *Crystal Growth*; Wiley: New York, 1951.
- (82) Sparks, R. A. et al. Operations Manual, Syntex P2₁ Diffractometer; Syntex Analytical Instruments: Cupertino, CA., 1972.
- (83) Sparks, R. A. et al. Operations Manual, Syntex XTL Structure Determination System; Syntex Analytical Instruments: Cupertino, CA., 1976.
- (84) Cooper, R. I.; Gould, R. O.; Parsons, S.; Watkin, D. J. The Derivation of Non-Merohedral Twin Laws During Refinement by Analysis of Poorly Fitting Intensity Data and the Refinement of Non-Merohedrally Twinned Crystal Structures in the Program *CRYSTALS*. *J. Appl. Crystallogr.* **2002**, *35*, 168–174.
- (85) Donnay, G.; Donnay, J. D. H. Classification of Triperiodic Twins. *Can. Mineral.* **1974**, *12*, 422–425.
- (86) Foxman, B. M. *OMEGA2*, A Program For Twinning Analysis and Prediction, 2020; <http://www.xray.chem.brandeis.edu>.
- (87) Rae, A. D. The use of partial observations, partial models and partial residuals to improve the least-squares refinement of crystal structures. *Crystallogr. Rev.* **2013**, *19*, 155–229.
- (88) Apex2, Version 2 User Manual, M86-E01078; *Bruker Analytical X-ray Systems*: Madison, WI, June 2006.